



ACCURATE PREDICTION OF NON-LINEAR WAVE FORCES: PART I (FIXED CYLINDER)

A. K. SWAIN AND S. A. BILLINGS

*Department of Automatic Control and Systems Engineering, University of Sheffield,
P.O. Box 600, Mappin Street, Sheffield, S1 3JD, U.K.*

AND

P. K. STANSBY

*Hydrodynamic Research Group, School of Engineering, University of Manchester,
Manchester, M13 9PL, U.K.*

AND

M. BAKER

Department of Civil Engineering, University of Salford, Salford, M7 1NU, U.K.

(Received March 1997, accepted after revisions October 1997)

A new equation structure is proposed as an alternative to the Morison equation for the prediction of wave forces. Initially, non-linear parametric continuous time differential equation models were estimated from wave force data for a variety of flow situations by adopting a new approach which avoids direct differentiation of the input–output data. The method consists of two stages. The first stage involves the estimation of a discrete time model (polynomial NARMAX) from sampled input–output data and computation of the linear and higher-order frequency response functions. The second stage involves identifying continuous time models by curve fitting to the complex frequency response data using a weighted complex orthogonal estimator. The orthogonal property of the estimator helps in identifying the correct model structure or which terms to include in the model, and the weighting property provides an additional degree of freedom to control the properties of the estimator with respect to the selection of the frequency range and number of data points. Morison equation models were fitted initially to the data but were shown to curve fit to the data without capturing the underlying dynamics. The frequency domain characteristics of the Morison equation models were also analysed and shown to be structurally deficient in representing certain dynamic features of the force. However, it is shown that the new equation structure is capable of emulating all the relevant features of the wave force mechanics. Extensive simulations on a variety of experimental data show that models based on the new structure perform remarkably well compared with the Morison equation. For each flow situation, in addition to the drag and inertia coefficients of the Morison equation, there are two non-dimensional coefficients defining history effects which show some consistency between widely different flow situations.

© 1998 Academic Press Limited

1. INTRODUCTION

An accurate and precise prediction of wave forces on offshore structures that are subjected to random ocean waves is an essential prerequisite for their design. Wave forces on structures composed of slender members are calculated traditionally on the basis of the

Morison equation which was introduced by Morison *et al.* [1] as a semi-intuitive expression predicting the force exerted on a body in a viscous fluid under unsteady flow conditions and is given by

$$\begin{aligned} F(t) &= \frac{1}{4}\pi\rho D^2 C_m \dot{u} + \frac{1}{2}\rho D C_d u |u| \\ &= K_i \dot{u} + K_d u |u| \end{aligned} \quad (1)$$

where $F(t)$ is the force per unit axial length, $u(t)$ is the instantaneous flow velocity, ρ is the water density, D is the diameter, $K_i = \frac{1}{4}\pi\rho D^2 C_m$, and $K_d = \frac{1}{2}\rho D C_d$. The dimensionless drag and inertia coefficients C_d and C_m depend on the characteristics of the flow. More recently the general validity of Morison's equation and particularly the validity in relation to wave-induced loads on circular cylinders has been questioned. Specifically the determination of C_d and C_m at high Reynolds numbers has presented a formidable problem that has endured for many years. Although much progress in the basic understanding of oscillatory flow has been made, many uncertainties and conditions in the reported data and conclusions still exist [2, 3]. The Morison equation generally predicts the main trends in measured data quite well; however, some characteristics of the flow are not well represented. For example in sinusoidal oscillatory flow, the force variation at the fundamental frequency may be well predicted while that at higher harmonics is not. This implies that peak forces may be poorly predicted. A poor representation of the high-frequency content of the forces is a serious limitation for the determination of the fatigue life of a structural element. Hence Morison's equation needs to be extended.

An attempt to determine new model structures to predict the wave forces has been made by Stansby *et al.* [4], who showed that two simple extended equations allow a considerable increase in the accuracy of curve fits to data measured in a variety of flow situations. A sophisticated system identification technique based on the non-linear autoregressive moving average with exogenous inputs (NARMAX) [5] model was used by Worden *et al.* [6] to model the wave force dynamics of U-tube, De Voorst and Christchurch Bay data. Although the discrete NARMAX models obtained could adequately represent the dynamics of the input-output data and performed well compared to the Morison equation so far as the predictive performance was concerned, the parameters of the discrete models could not be easily related to the physical parameters of the inherently continuous time system. Hence, it is often desirable to fit continuous time models to the input-output data to obtain physically interpretable parameters.

Identification of continuous time models from input-output data has been studied by several authors in the past and comprehensively documented by Unbehauen and Rao [7]. Most of the techniques developed so far are limited to the identification of linear systems and make use of several types of modulating functions, state variable filters, Poisson filter chains and chain integrators in order to avoid direct differentiation of the process data. Extending these techniques to the identification of non-linear systems is much more complicated.

An alternative indirect approach is to estimate the parameters of a continuous time differential equation model by curve fitting to the system frequency response functions. However, when the system is non-linear, computation of the higher-order frequency response functions directly from input-output data involves extending the classical cross- and power spectral density concepts to multidimensions and using correlation- or FFT (fast fourier transform)-based techniques coupled with multidimensional windowing and smoothing [8]. An indirect approach is to estimate a linear or non-linear discrete time model from sampled input-output data and then to compute the higher-order frequency

response functions from the unbiased process model using the recursive algorithm proposed in [9, 10]. The latter approach offers significant advantages since only small data sets are required and the complexities of multidimensional windowing and smoothing are avoided.

The present study attempts to find continuous time models which accurately represent the non-linear wave force data by parameterising the system frequency response functions in terms of the coefficients of a non-linear ordinary differential equation [11, 12]. The motivation for this approach comes from the fact that the discrete representation of a continuous time system is not unique. Thus different discrete time models can be obtained for the same system. But whatever models are obtained, if the models have captured the dynamics of the system adequately, the frequency response functions must be the same. Therefore, the present method utilises the invariant information in the frequency response functions to fit continuous time models. The procedure consists of three steps:

- identify a discrete time model (polynomial NARMAX) using sampled input–output data;
- compute the linear and non-linear frequency response functions using the algorithms of [9, 10];
- identify the continuous time models by curve fitting to the frequency response functions using the weighted complex orthogonal estimator [12].

Based on the observations of the experimental data and from preliminary mathematical analysis of the Morison equation, a new equation structure is proposed for prediction of wave forces.

The organisation of the paper is as follows. Section 2 highlights the preliminary characteristics of the Morison equation. A brief tutorial concerning the concepts and techniques of fitting discrete parametric models (NARMAX) from sampled input–output data is presented in Section 3. The concept of frequency domain analysis and the interpretation of generalised frequency response functions (GFRF) are briefly introduced in Section 4. The procedure of identifying non-linear continuous time differential equation models from complex frequency response data using the weighted complex orthogonal estimator is described in Section 5. The identification of non-linear differential equation models from several data sets is carried out in Sections 6–8. Section 9 analyses further the behaviour of the Morison equation from the point of view of system identification, and a new equation structure is proposed for the prediction of wave forces. Continuous time models are fitted based on the proposed structure using least squares.

2. FREQUENCY DOMAIN CHARACTERISTICS OF MORISON'S EQUATION

Since the final objective of this study is to fit non-linear continuous time models of the wave forces, it is appropriate to begin by analysing the general behaviour of the Morison equation. A comparative analysis of the Morison model and the discrete NARMAX model for specific sets of data has been made in the practical examples.

It is not possible to map directly the Morison equation into the frequency domain using the techniques of Volterra series due to the presence of the drag term $u|u|$ which has a discontinuous second derivative, since a necessary condition for the existence of the Volterra series is that all non-linearities must be infinitely differentiable [13]. However, it is possible to approximate the drag term $u|u|$ in equation (1) as a polynomial of the form

$$u|u| = a_1u + a_2u^2 + a_3u^3 + a_4u^4 + a_5u^5 + \cdots \quad (2)$$

Under the assumption that the input signal is a zero-mean Gaussian signal whose odd-order moments are identically zero (often a reasonable assumption), equation (2) can be represented as an odd-order polynomial of the form

$$u|u| = a_1u + a_3u^3 + a_5u^5 + \cdots \quad (3)$$

Therefore, the approximated Morison equation is given by

$$\begin{aligned} F(t) &= K_i\dot{u} + K_d(a_1u + a_3u^3 + a_5u^5 + \cdots) \\ &= K_i\dot{u} + K_{d1}u + K_{d3}u^3 + K_{d5}u^5 + \cdots \end{aligned} \quad (4)$$

where $K_{d1} = K_d a_1$, $K_{d3} = K_d a_3$, and so on. The analysis of the approximated Morison equation is possible using techniques of the Volterra series. Assuming that the drag term can be approximated with reasonable accuracy by a third-order polynomial of the input, the approximated Morison equation is given by

$$F(t) = K_i\dot{u} + K_{d1}u + K_{d3}u^3. \quad (5)$$

The linear and third-order transfer functions of the approximated Morison equation of equation (5) are given by

$$H_1(j\omega_1) = K_{d1} + j\omega_1 K_i \quad (6)$$

$$H_3(j\omega_1, j\omega_2, j\omega_3) = K_{d3}. \quad (7)$$

From the linear transfer function [equation (6)], it is obvious that as $\omega_1 \rightarrow \infty$, the magnitude $|H_1(j\omega_1)| \rightarrow \infty$ which means that when the cylinder is subjected to a high-frequency input wave of very small amplitude, it will experience an extremely high force. The third-order frequency response function is a constant independent of the frequency of the input wave.

The intrinsic characteristic of the Morison equation is such that it can adequately capture the dynamics of a system whose linear gain increases with the frequency of the input signal (as evident from its linear transfer function). However, in the case of most practical systems, the gain of the system falls off as the frequency increases. It is obvious in the examples when models are fitted to the real data that Morison's equation may require modification and extension.

The first step in the search for a possible extension of the Morison equation is to fit continuous time models to the input–output (velocity inline force) data for a variety of flow situations and look for any consistency in the models. However, the estimation of continuous time differential equation models from raw input–output data involves differentiation of the data and hence may result in incorrect parameter estimates due to the presence of noise inherent in practical data. To avoid errors due to differentiation, a new approach is followed in the estimation process where a discrete NARMAX model is fitted initially to the data and then continuous time models are fitted to the frequency response functions which are computed from the NARMAX model. Note that one of the most important advantages of the NARMAX model is that the process terms and noise terms are decoupled from each other; thus, the computed frequency response functions from the process model are noise free.

Prior to the estimation of continuous time models, the relevant theoretical prerequisites of the procedure adopted in the estimation phase are briefly presented in tutorial form in Sections 3–5.

3. SYSTEM IDENTIFICATION IN THE DISCRETE DOMAIN—THE POLYNOMIAL NARMAX MODEL

The problem of system identification is concerned primarily with the mathematical representation of a linear or non-linear input output relationship. The mathematical model representation basically depends on the identification methods considered and the structure of the data that are available. The identification of non-linear systems using the functional series expansion of Volterra and related methods have been comprehensively documented by Billings [14]. The representation of a non-linear system by the functional series expansion of Volterra or Wiener that maps past inputs into the present outputs requires an excessive parameter set often in excess of 500 kernel values, even for simple non-linear systems, and hence proves to be impractical.

However, the difficulty of excessive parameters associated with the Volterra modelling of non-linear systems can be overcome by representing the system by a discrete parametric model. One of the possible choices is the NARMAX model, initially proposed by Billings and Leonatartitis [15]. It has been proved by Leontaritis and Billings [5], that a non-linear discrete-time time invariant system can always be represented by the NARMAX model

$$y(k) = F^{N_l}[y(k-1), \dots, y(k-n_y), u(k-1), \dots, u(k-n_u), e(k-1), \dots, e(k-n_e)] + e(k) \quad (8)$$

in a region around an equilibrium point provided the response function of the system is finitely realisable and a linearised model would exist if the system were to be operated close to the chosen equilibrium point, where $y(k)$, $u(k)$ and $e(k)$ represent the output, input and noise respectively at time intervals k , n_y , n_u , n_e are the corresponding lags, and $F^{N_l}[\cdot]$ is some non-linear function. In practice, the noise $e(k)$ cannot usually be measured and is replaced by the prediction errors defined as

$$\varepsilon(k) = y(k) - \hat{y}(k) \quad (9)$$

where $\hat{y}(k)$ is the one-step-ahead prediction of $y(k)$.

It should be noted that the model includes both linear and non-linear noise components. If the system is non-linear, any noise that arises is also likely to be non-linear. Although all these terms correspond to unmeasurable states, they must be included in the model, otherwise the estimated parameters will contain systematic errors called bias.

3.1. STRUCTURE DETECTION AND PARAMETER ESTIMATION

In the present study, the map $F^{N_l}[\cdot]$ is taken to be a polynomial of degree N_l , but $F^{N_l}[\cdot]$ can be defined as a neural network, rational function expansion, etc. In order to estimate the parameters of this map, equation (8) is expressed in prediction error form as

$$y(k) = \sum_{i=1}^{N_l} \theta_i x_i(k) + e(k) \quad (10)$$

where N_l is maximum number of terms in the NARMAX model and is given by

$$N_l = \sum_{i=0}^{N_l} n_i \quad n_0 = 1$$

$$n_i = n_{i-1}(n_y + n_u + n_e + i - 1)/i, \quad i = 1, \dots, N_l \quad (11)$$

and

$$x_1(k) = 1$$

$$x_i(k) = \prod_{j=1}^{p_y} y(k - n_{y_j}) \prod_{k=1}^{q_u} u(k - n_{u_k}) \prod_{m=1}^{r_e} e(k - n_{e_m}) \quad (12)$$

where $i = 2, \dots, n$; $p_y, q_u, r_e \geq 0$; $1 \leq p_y + q_u + r_e \leq N_i$; $1 \leq n_{y_j} \leq n_y$; $1 \leq n_{u_k} \leq n_u$; $1 \leq n_{e_m} \leq n_e$; and N_i is the degree of polynomial expansion.

By convention, $p_y = 0$ indicates that $x_i(k)$ contains no $y(\cdot)$ terms. Similarly $q_u = 0$ indicates that $x_i(k)$ contains no $u(\cdot)$ terms and $r_e = 0$ indicates that $x_i(k)$ contains no $e(\cdot)$ terms. Regrouping terms in equation (8) yields

$$y(k) = F^p[y(k-1), \dots, y(k-n_y), u(k-1), \dots, u(k-n_u)]$$

$$+ F^n[y(k-1), \dots, y(k-n_y), u(k-1), \dots, u(k-n_u), e(k-1), \dots, e(k-n_e)] + e(k) \quad (13)$$

where $F^p[\cdot]$ contains all terms $\theta_i x_i(k)$ with $r_e = 0$, and $F^n[\cdot]$ contains all terms $\theta_i x_i(k)$ with $r_e \neq 0$. $F^p[\cdot]$ is referred to as the process model and $F^n[\cdot]$ as the noise model. When the system is non-linear, direct estimation based on equation (13) may involve an excessive number of terms. Simply increasing the orders n_y , n_u and n_e and the degree N_i of the polynomial expansion to achieve the desired accuracy in general will result in an excessively complex model and possibly numerical ill-conditioning. The determination of the structure or which terms to include in the model is therefore essential if a parsimonious model is to be determined from the large number of candidate terms [equation (11)]. An orthogonal regression estimator [16] can select a subset of significant terms very efficiently. The basic idea is to transfer the model of equation (13) into an equivalent orthogonal equation. Because of the orthogonal property, significant terms can be determined in a particularly simple forward regression procedure. The criterion for selecting terms is based upon the proportion of the output variance that each term contributes.

An advantage of the orthogonal estimator is that significant parameters can be determined recursively and quite independently of the other terms already selected. Furthermore, the estimation of the process and noise model parameters can be decoupled. This is particularly useful for the identification of the model of equation (13). A parsimonious process model is first determined. This model is not affected by whatever noise model is produced later. The initial prediction errors are computed based on this process model and a noise model can then be selected. A revised prediction error sequence is then calculated and an improved noise model is determined.

3.2. MODEL VALIDITY TESTS

After fitting a NARMAX model to the input–output data, it is important to test for possible inadequacies of the fitted model, i.e. to check if the model has successfully captured the system dynamics and is not just a curve fit to one data set. The problems of curve fitting are discussed in the examples. Over the last few years, much work has been reported relating to the design and development of model validation tools [17, 18]. In the present study, the models are validated based on the predictive performance (cross-validation) and correlation tests.

3.2.1. Cross-validation

One technique which can be used to judge the qualitative performance of a model is to assess the predictive performance based on both one-step ahead prediction of the system output defined as

$$\hat{y}_{osa}(k) = F^{N_l}[y(k-1), \dots, y(k-n_y), u(k-1), \dots, u(k-n_u), e(k-1), \dots, e(k-n_e)] \quad (14)$$

and the model predicted output given by

$$\hat{y}_{mpo}(k) = F^{N_l}[\hat{y}_{mpo}(k-1), \dots, \hat{y}_{mpo}(k-n_y), u(k-1), \dots, u(k-n_u)] \quad (15)$$

A metric which measures the closeness of fit between the predicted output and measured output is the normalised root mean square error (NMSE) which is defined as [19]

$$NMSE = \sqrt{\frac{\sum (\hat{y}(k) - y(k))^2}{\sum (y(k) - \bar{y})^2}} \quad (16)$$

where $\hat{y}(k)$ is the predicted (either one-step-ahead or model predicted) output of the system. Another approach commonly known as cross-validation, is based on dividing the available data set into two disjoint sets, the estimated and the test set. The former is used for estimation and the latter set is used for model validation.

3.2.2. Correlation tests

The classical approach to validating identified linear models consists of computing the autocorrelation function of the residuals and the cross-correlation function between the residuals and the input [20]. This result has been extended by [17, 18] workers to the case of validating identified non-linear models. The identified model produces acceptable predictions over different data sets only if it is unbiased. If the model structure and the estimated parameters are correct, then the prediction error sequence $\varepsilon(k)$ should be unpredictable from all linear and non-linear combinations of past inputs and outputs. This condition will hold if and only if the following conditions hold

$$\begin{aligned} \phi_{\varepsilon\varepsilon}(\tau) &= E[(\varepsilon(k-\tau)\varepsilon(t))] = \delta(\tau), \\ \phi_{ue}(\tau) &= E[u(k-\tau)\varepsilon(t)] = 0, \quad \forall \tau, \\ \phi_{[uu]'\varepsilon}(\tau) &= E[(u^2(k-\tau) - \overline{u^2(t)})\varepsilon(t)] = 0, \quad \forall \tau, \\ \phi_{[uu]'\varepsilon^2}(\tau) &= E[(u^2(k-\tau) - \overline{u^2(t)})\varepsilon^2(t)] = 0, \quad \forall \tau, \\ \phi_{(\varepsilon)[uu]}(\tau) &= E[\varepsilon(t)\varepsilon(k-1-\tau)u(k-1-\tau)] = 0, \quad \tau \geq 0, \end{aligned} \quad (17)$$

where $\delta(\tau)$ is the Kronecker delta, the bar signifies mean value, and $E[\cdot]$ denotes expectation. The underlying rationale of the correlation tests is that for a model to be statistically valid, there should be no predictable information in the residuals. However, in practice only a finite data length is available which is contaminated with noise (which is rarely additive, Gaussian or white) measured with finite precision and subject to innumerable external influences in the environment and the measurement apparatus. Hence, confidence bands should be used to indicate if the correlation between variables is significant or not. For large N , the 95% confidence bands are approximately $\pm 1.96/\sqrt{N}$

and any significant correlation will be indicated by points lying outside the respective confidence band.

3.3. PREPROCESSING OF THE DATA

Before estimation, the raw data may require preprocessing, e.g. removal of any possible trends in the data and suitable choice of sampling time, in order to avoid possible numerical ill-conditioning and identifiability problems.

3.3.1. Choice of sampling time

A good choice of sampling time is central to the success of any identification algorithm. Many studies have been made for selecting proper sampling times for identifying and controlling linear systems [21, 22]. The sampling time should be neither too small nor too large. Too small a sampling time causes the data vector to be autocorrelated and hence involves singularity of the information matrix. Too large a sampling time can cause a loss of information, i.e. the inter-sample behaviour contains a lot of information. All previous observations are based on a rule of thumb: for successful control and identification of a linear system, the sampling time T_s should lie between $\frac{1}{10}$ th and $\frac{1}{20}$ th of the dominant time constant of the system or at least 15–20 samples should be taken between 95% of the settling time of the system.

The choice of sampling times for non-linear systems has received relatively little attention in the past until recently when Billings and Aguirre [23] showed that the sampling time which enhances model structure selection is not necessarily the best choice of sampling time for parameter estimation and vice versa. Billings and Aguirre [23] suggested several rules for selecting the sampling time but the most practical and easiest method is to analyse the linear and non-linear correlation functions of the output. Consider the correlation functions

$$\begin{aligned}\phi_{yy}(\tau_c) &= E[(y(k) - \overline{y(k)})(y(k - \tau_c) - \overline{y(k)})] \\ \phi_{y^2y^2}(\tau_c) &= E[(y^2(k) - \overline{y^2(k)})(y^2(k - \tau_c) - \overline{y^2(k)})], \quad \tau_c = 0, 1, \dots\end{aligned}\quad (18)$$

Then determine

$$\tau_m = \min [\tau_y, \tau_{y^2}] \quad (19)$$

where τ_y is the time of the first minimum of $\phi_{yy}(\tau)$ and τ_{y^2} is defined analogously. Finally the sampling time can be chosen as $\tau_m/20 \leq T_s \leq \tau_m/10$.

It should be emphasised here that the above procedure only provides a guide to the selection of sampling time. The choice differs from process to process and upon the individual requirements.

4. FREQUENCY DOMAIN ANALYSIS AND INTERPRETATION

In the last section, procedures for fitting discrete NARMAX models were discussed. However, the discrete polynomial NARMAX representation of a particular system is not necessarily unique which means that it is possible to obtain different discrete models for the same system. Thus, one cannot be certain that the difference in model structure is due to differences in the underlying physics, or if it is simply a reflection of non-uniqueness. However, no matter what the form of the model, if the model correctly captures the dynamics associated with the data sufficiently, this must reflect the correct linear and non-linear frequency content of the system. In other words, although there may be a

number of discrete time models that represent a continuous time system, the higher-order frequency response functions corresponding to each of the discrete models should correspond with those for the continuous time system description. This forms the motivation for analysing the above systems in the frequency domain.

Since continuous time differential equation models are to be estimated for different sets of wave force data by curve fitting to the GFRF (computed by mapping the NARMAX models into the frequency domain), a brief review of this is given below.

The n th order GFRF of a system is defined as

$$H_n(j\omega_1, \dots, j\omega_n) = \int_{-\infty}^{\infty} \dots \int_{-\infty}^{\infty} h_n(\tau_1, \dots, \tau_n) e^{(-j(\omega_1\tau_1 + \dots + \omega_n\tau_n))} d\tau_1 \dots d\tau_n \quad (20)$$

where $h_n(\tau_1, \dots, \tau_n)$ is known as the n th-order Volterra Kernel or generalised impulse response function of order n . The frequency domain representation of a system having non-linearity of degree N_l is given as

$$\begin{aligned} Y(j\omega) &= \sum_{n=1}^{N_l} Y_n(j\omega) \\ &= \sum_{n=1}^{N_l} \frac{1}{2\pi^{n-1}} \int_{-\infty}^{\infty} \dots \int_{-\infty}^{\infty} H_n(j\omega_1, \dots, j\omega_n) U(j\omega_1) \dots U(j\omega_n) d\omega_1 \dots d\omega_{n-1} \end{aligned} \quad (21)$$

where $\omega = \omega_1 + \omega_2 + \dots + \omega_n$, $Y(j\omega)$ and $U(j\omega)$ represent spectrum of output and input, respectively.

For example, if a system were represented by a Volterra series of order 3, then

$$\begin{aligned} Y(j\omega) &= H_1(j\omega_1)U(j\omega_1) + \frac{1}{2\pi} \int_{-\infty}^{\infty} H_2(j\omega_1, j\omega_2)U(j\omega_1)U(j\omega_2) d\omega_1 \\ &\quad + \frac{1}{(2\pi)^2} \int_{-\infty}^{\infty} \int_{-\infty}^{\infty} H_3(j\omega_1, j\omega_2, j\omega_3)U(j\omega_1)U(j\omega_2)U(j\omega_3) d\omega_1 d\omega_2. \end{aligned} \quad (22)$$

4.1. RELEVANT FREQUENCIES OF THE GFRT PLOTS

An important property of non-linear systems is that new frequencies may be generated in the output including harmonics and intermodulation effects caused by the non-linear interaction and mixing of input frequency components. These phenomena are captured by the GFRF.

If a system possessing an n th-order non-linear term is excited by an input signal that is strictly band-limited such that it has no spectral components above some frequency $(\omega_u)_{max}$, the maximum frequency $(\omega_y)_{max}$ of the output will contain n th-order harmonics of the highest frequency of the input and thus will satisfy the relation

$$(\omega_y)_{max} = n(\omega_u)_{max}. \quad (23)$$

Therefore, the sampling frequency ω_s must satisfy the following inequalities to avoid aliasing

$$\begin{aligned} \omega_s &\geq 2 \times (\omega_y)_{max}, \\ &\geq 2 \times n(\omega_u)_{max}. \end{aligned} \quad (24)$$

Furthermore, the n th-order GFRF $H_n(j\omega_1, \dots, j\omega_n)$, which is a multidimensional function will generate an intermodulation frequency $\omega = \omega_1 + \dots + \omega_n$ in the output for a particular combination $(\omega_1, \dots, \omega_n)$ in the input frequency space. Since input–output signals are sampled at the sampling frequency ω_s , only those frequencies within the fundamental range $[-\omega_s/2, \omega_s/2]$ are meaningful. Hence it is required that $\omega = \omega_1 + \dots + \omega_n$ should be kept within the fundamental frequency range. Since each frequency variable $\omega_1, \dots, \omega_n$ in the n -tone input varies independently, the relevant range for the n th-order frequency response function $H_n(j\omega_1, \dots, j\omega_n)$ is $\omega_i \leq \omega_s/2n$. The value of the GFRF beyond this frequency range should be ignored therefore.

4.2. INTERPRETATION OF GFRF

The GFRF of discrete NARMAX models can be obtained using the recursive algorithm of Peyton Jones and Billings [10]. The frequency at which the magnitude of the linear transfer function $H_1(j\omega_1)$ is maximum is the linear resonant frequency of the system (say, ω_r). This indicates that for this frequency of excitation, the amplitude of the linear part of the response $y_1(t)$ is a maximum. Similarly, it is possible to interpret the higher-order frequency response functions from the magnitude and contour plots. For example, the ridges in the contour plot of the higher-order frequency response functions are equivalent to the peaks in the linear frequency response plot $H_1(j\omega_1)$. Thus, if the equation of the ridge in the n th-order transfer function is given by $\omega_1 + \omega_2 + \dots + \omega_n = \omega_{nlr}$, this indicates that the n th-order output $y_n(t)$ of the system will be a maximum if the system is excited by an input whose frequency sum equals ω_{nlr} .

To improve further the understanding and interpretation of the generalised frequency response plots, consider as an example a system which is modelled by the NARMAX model of the form

$$y(k) = a_1 y(k-1) + a_2 y(k-2) + b_1 u(k-1) + b_2 u(k-2) + c_1 u(k-1)u(k-2)u(k-3). \quad (25)$$

The linear transfer function of this system is given by

$$\begin{aligned} H_1(j\omega_1) &= (b_1 e^{-j\omega_1} + b_2 e^{-j2\omega_1}) \cdot \frac{1.0}{1 - a_1 e^{j\omega_1} - a_2 e^{-j2\omega_1}} \\ &= H_1^{(MA)}(j\omega_1) \cdot H_1^{(AR)}(j\omega_1) \end{aligned} \quad (26)$$

where $H_1^{(MA)}(j\omega_1)$ corresponds to the part of the linear transfer function due to pure input terms only (moving average part), and $H_1^{(AR)}(j\omega_1)$ corresponds to the part of $H_1(j\omega_1)$ due to pure linear output terms (autoregressive part).

Since the model does not possess any second-order non-linear terms, the second-order transfer function $H_2(j\omega_1, j\omega_2)$ is absent. The analytical expression for the third-order frequency response function of the system is given by

$$H_3(j\omega, j\omega_2, j\omega_3) = \frac{c_1 e^{-j(\omega_1 + 2\omega_2 + 3\omega_3)}}{1 - a_1 e^{-j(\omega_1 + \omega_2 + \omega_3)} - a_2 e^{-j2(\omega_1 + \omega_2 + \omega_3)}}. \quad (27)$$

Note that for the present case, the contribution of the non-linear term to the magnitude of $H_3(\cdot)$ is c_1 since the magnitude of the phasor remaining in the numerator of $H_3(\cdot)$ is unity. Comparing the expression for $H_3(\cdot)$ with that of $H_1^{(AR)}(\cdot)$ in equation (26), it will be obvious that if ω_r^{AR} is the resonant frequency of $H_1^{(AR)}(\cdot)$, the maximum in the magnitude of $H_3(\cdot)$ will occur when $\omega_1 + \omega_2 + \omega_3 = \omega_r^{AR}$. Thus if a system possesses pure input non-linearity, the peak in the magnitude of $H_3(\cdot)$ will occur at those combinations of input frequencies whose sum equals the resonant frequency of the autoregressive part of the linear transfer function.

5. RECONSTRUCTION OF NON-LINEAR CONTINUOUS TIME MODELS

Before a non-linear continuous time model can be fitted to the frequency response data the form of the general non-linear continuous time model must be defined. Consider a system whose dynamics are described by the non-linear differential equation

$$\sum_{m=1}^{N_l} \sum_{p=0}^m \sum_{l_1, l_p+q=0}^L c_{p,q}(l_1, \dots, l_{p+q}) \prod_{i=1}^p D^{l_i} y(t) \prod_{i=p+1}^{p+q} D^{l_i} u(t) = 0 \quad (28)$$

where L is the maximum order of the differential, N_l is the maximum degree of nonlinearity, and $p+q=m$ and $m=1, \dots, N_l$ correspond to various orders of non-linearity. The operator D is the differential operator. Once m takes a specific number, all the m th-order terms, each of which contains a p th-order factor in $D^{l_i} y(t)$ and a q th-order factor in $D^{l_i} u(t)$ subject to $p+q=m$, are included and each term is multiplied by a coefficient $c_{p,q}(l_1, \dots, l_{p+q})$, while the multiple summation over the $l_i (l_i = 0 \dots L)$ generates all possible permutations of differentiations. For example, the general linear differential equation is included in the above form by setting the order of non-linearity m as 1 to give:

$$\sum_{l_1=0}^L c_{1,0}(l_1) D^{l_1} y(t) + \sum_{l_1=0}^L c_{0,1}(l_1) D^{l_1} u(t) = 0. \quad (29)$$

As an example, the differential equation

$$\frac{d^2 y}{dt^2} + 2.5 \frac{dy}{dt} + 1.0y + 1.2 \frac{du}{dt} + u + 100y^2 + 50u^2 + 10^4 y^3 + 25.0 \left(\frac{dy}{dt} \right) u^2 = 0 \quad (30)$$

would be represented by the model of equation (28) with following definitions: $c_{1,0}(0) = 1.0$, $c_{1,0}(1) = 2.5$, $c_{1,0}(2) = 1.0$, $c_{0,1}(0) = 1.0$, $c_{0,1}(1) = 1.2$, $c_{2,0}(0, 0) = 100.0$, $c_{0,2}(0, 0) = 50.0$, $c_{3,0}(0, 0, 0) = 10^4$, and $c_{1,2}(1, 0, 0) = 25.0$.

The frequency domain equivalent of equation (28) is based on the GFRF which are given by mapping the time domain representation into the frequency domain

$$\begin{aligned} & - \left[\sum_{l_1=0}^L c_{1,0}(l_1) (j\omega_1 + \dots j\omega_n)^{l_1} \right] H_n^{asym}(j\omega_1, \dots j\omega_n) \\ & = \sum_{l_1, l_n=0}^L c_{0,n}(l_1, \dots l_n) (j\omega_1)^{l_1} \dots (j\omega_n)^{l_n} \\ & + \sum_{q=1}^{n-1} \sum_{p=1}^{n-q} \sum_{l_1, l_p=0}^L c_{p,q}(l_1, \dots l_{p+q}) (j\omega_{n-q+1})^{l_{p+1}} \dots (j\omega_n)^{l_{p+q}} H_{n-q,p}(j\omega_1, \dots j\omega_{n-q}) \\ & + \sum_{p=2}^n \sum_{l_1, l_p=0}^L c_{p,0}(l_1, \dots l_p) H_{n,p}(j\omega_1, \dots j\omega_n) \end{aligned} \quad (31)$$

where the recursive relation is given by

$$H_{n,p}^{asym}(\cdot) = \sum_{i=1}^{n-p+1} H_i(j\omega_1, \dots j\omega_i) H_{n-i,p-1}(j\omega_{i+1}, \dots j\omega_n) (j\omega_1 + \dots + j\omega_i)^{l_p}. \quad (32)$$

The recursion finishes with $p = 1$, and $H_{n,1}(j\omega_1, \dots, j\omega_n)$ has the property

$$H_{n,1}(j\omega_1, \dots, j\omega_n) = H_n(j\omega_1, \dots, j\omega_n)(j\omega_1 + \dots + j\omega_n)^{l_1}. \quad (33)$$

The above equations for the GFRF are used to derive the regression equations for estimating the unknown parameters $c_{p,q}(l_1, \dots, l_{p+q})$ in equation (34).

Note that the computation of the n th-order frequency response functions is a recursive procedure where each lower order of the GFRF contains no effects from higher-order terms. This offers a distinct advantage since the parameters corresponding to different non-linearities or terms in the continuous time non-linear differential equation can be estimated one at a time and quite independently, beginning with first-order terms and then building up to include the non-linear terms.

5.1. ESTIMATION OF LINEAR TERMS

The first-order frequency response is only related to the linear input-output terms. Setting $n = 1$ in equation (31) gives

$$-\left[\sum_{l_1=0}^L c_{1,0}(l_1)(j\omega_1)^{l_1} \right] H_1(j\omega_1) = \sum_{l_1=0}^L c_{0,1}(l_1)(j\omega_1)^{l_1}. \quad (34)$$

Without loss of generality, it is assumed that the parameter corresponding to the linear output term $c_{1,0}(0)$ is unity. Moving all other terms to the right-hand side gives

$$-H_1(j\omega_1) = \sum_{l_1=1, l_1 \neq 0}^L c_{1,0}(l_1)(j\omega_1)^{l_1} H_1(j\omega_1) + \sum_{l_1=0}^L c_{0,1}(l_1)(j\omega_1)^{l_1} \quad (35)$$

which is linear in the parameters expression. The parameters $c_{1,0}(\cdot)$ and $c_{0,1}(\cdot)$ can be estimated using the weighted complex orthogonal estimator [12] (described in Appendix A). For clarity, compare equation (35) and (A1) to relate the parameters of both equations.

So, from equation (A1)

$$\begin{aligned} z(j\omega) &= \theta_1 p_1(j\omega) + \theta_2 p_2(j\omega) + \dots + \theta_M p_M(j\omega) \\ z(j\omega) &= -H_1(j\omega_1) \\ \theta_1 &= c_{1,0}(1), \quad p_1(j\omega) = (j\omega_1) H_1(j\omega_1) \\ \theta_2 &= c_{1,0}(2), \quad p_2(j\omega) = (j\omega_1)^2 H_1(j\omega_1) \\ &\vdots \\ \theta_L &= c_{1,0}(L), \quad p_L(j\omega) = (j\omega_1)^L H_1(j\omega_1) \\ \theta_{L+1} &= c_{0,1}(0), \quad p_{L+1}(j\omega) = (j\omega_1)^0 = 1 \\ \theta_{L+2} &= c_{0,1}(1), \quad p_{L+2}(j\omega) = (j\omega_1) \\ \theta_{L+3} &= c_{0,1}(2), \quad p_{L+3}(j\omega) = (j\omega_1)^2 \\ &\vdots \\ \theta_{2L+1} &= c_{0,1}(L), \quad p_{2L+1}(j\omega) = p_M(j\omega) = (j\omega_1)^L. \end{aligned} \quad (36)$$

The proposed estimation algorithm can now be applied to equation (36) to identify the unknown parameters by replacing the frequency response function $H_1(j\omega_1)$ by estimates of this function.

5.2. ESTIMATION OF SECOND-ORDER NON-LINEARITIES

To estimate the parameters associated with second-order non-linear terms, set $n = 2$ in equation (31) so that

$$\begin{aligned}
 -\left[\sum_{l_1=0}^L c_{1,0}(l_1)(j\omega_1 + j\omega_2)^{l_1} \right] H_2^{asym}(j\omega_1, j\omega_2) &= \sum_{l_1, l_2=0}^L c_{0,2}(l_1, l_2)(j\omega_1)^{l_1}(j\omega_2)^{l_2} \\
 &+ \sum_{l_1, l_2=0}^L c_{1,1}(l_1, l_2)(j\omega_2)^{l_2} H_{1,1}(j\omega_1) \\
 &+ \sum_{l_1, l_2=0}^L c_{2,0}(l_1, l_2) H_{2,2}(j\omega_1, j\omega_2).
 \end{aligned} \tag{37}$$

By the recursive relation

$$H_{1,1}(j\omega_1) = H_1(j\omega_1)(j\omega_1)^{l_1}, \tag{38}$$

$$\begin{aligned}
 H_{2,2}^{asym}(j\omega_1, j\omega_2) &= H_1(j\omega_1) H_{1,1}(j\omega_2)(j\omega_1)^{l_2} \\
 &= H_1(j\omega_1) H_1(j\omega_2)(j\omega_2)^{l_1}(j\omega_1)^{l_2}.
 \end{aligned} \tag{39}$$

So that finally a linear regression equation is obtained as

$$\begin{aligned}
 -\left[\sum_{l_1=0}^L c_{1,0}(l_1)(j\omega_1 + j\omega_2)^{l_1} \right] H_2^{asym}(j\omega_1, j\omega_2) &= \sum_{l_1, l_2=0}^L c_{0,2}(l_1, l_2)(j\omega_1)^{l_1}(j\omega_2)^{l_2} \\
 &+ \sum_{l_1, l_2=0}^L c_{1,1}(l_1, l_2)(j\omega_2)^{l_2} H_1(j\omega_1)(j\omega_1)^{l_1} \\
 &+ \sum_{l_1, l_2=0}^L c_{2,0}(l_1, l_2) H_1(j\omega_1) H_1(j\omega_2)(j\omega_1)^{l_2}(j\omega_2)^{l_1}.
 \end{aligned} \tag{40}$$

Notice that the parameters $c_{1,0}(l_1)$, $l_1 = 0, \dots, L$ on the left-hand side have been estimated as linear terms initially while all the parameters on the right-hand side can be estimated from equation (37) by replacing the first- and second-order frequency response functions by their estimates and applying the estimator.

5.3. ESTIMATION OF HIGHER-ORDER NON-LINEARITIES

When dealing with higher-order terms ($n = 3, 4, \dots$), some parameters which have been obtained in previous stages (for orders less than the n th) appear on the right-hand side

of the equation. These are associated with lower-order pure output and cross-product terms but not pure input terms. Moving these terms to the left-hand side gives

$$\begin{aligned}
& - \left[\sum_{l_1=0}^L c_{1,0}(l_1)(j\omega_1 + \dots j\omega_n)^{l_1} \right] H_n^{asym}(j\omega_1, \dots j\omega_n) \\
& - \sum_{q=1}^{n-2} \sum_{p=1}^{n-q-1} \sum_{l_1, l_n=0}^L c_{p,q}(l_1, \dots l_{p+q})(j\omega_{n-q+1})^{l_{p+1}} \dots (j\omega_n)^{l_{p+q}} H_{n-q,p} \\
& \times (j\omega_1, \dots j\omega_{n-q}) - \sum_{p=2}^{n-1} \sum_{l_1, l_p=0}^L c_{p,0}(l_1, \dots l_p) H_{n,p}(j\omega_1, \dots j\omega_n) \\
& = \sum_{l_1, l_n=0}^L c_{0,n}(l_1, \dots l_n)(j\omega_1)^{l_1} \dots (j\omega_n)^{l_n} \\
& + \sum_{q=1}^{n-1} \sum_{l_1, l_n=0}^L c_{p,q}(l_1, \dots, l_n)(j\omega_{n-q+1})^{l_{p+1}} \dots (j\omega_n)^{l_{p+q}} H_{n-q,n-q}(j\omega_1, \dots, j\omega_{n-q}) \\
& + \sum_{l_1, l_n=0}^L c_{n,0}(l_1, \dots, l_p) H_{n,n}(j\omega_1, \dots, j\omega_n). \tag{41}
\end{aligned}$$

The reconstruction is achieved by applying the weighted complex orthogonal estimator (Appendix A). Full details of the algorithm, the properties and guidelines for implementation can be found in [12]. The weighting matrix Q in all the examples has been taken to be

$$Q = \text{diag} [q_1(\omega), q_2(\omega), \dots q_N(\omega)] \tag{42}$$

where $q_i(\omega)$ is a monotonically decreasing exponential of the form

$$q_i = e^{(-\omega_{i|\lambda}^2)}. \tag{43}$$

The weighting parameter λ controls the distribution of the weights of the errors for each frequency ω .

In the following sections, wave force data from a variety of systems have been modelled by applying the techniques and procedures described in previous sections. In all the examples the models have been fitted and analysed in the following manner:

- fit a discrete NARMAX model to the sampled input–output data by applying an orthogonal least squares (OLS) estimator;
- compute and interpret the generalised frequency response functions of the estimated NARMAX model;
- fit a Morison equation model to the input–output data using conventional least squares curve-fitting techniques and make a comparative analysis with respect to the NARMAX model;
- estimate non-linear continuous time differential equation models by curve fitting to the GFRF.

TABLE 1
Experimental conditions of the Salford cylinder

Data set	Minimum frequency (Hz)	Maximum frequency (Hz)	Spectral bandwidth (Hz)	Sampling interval (s)	No. of data collected	Flow parameters		
						KC	β	Re
1	0.3239	0.6002	0.2763	0.02	20 972	4.74	667.2	$3.1638\text{E} + 03$
2	0.2570	0.6476	0.3906	0.02	19 437	4.95	653.11	$3.2332\text{E} + 03$
3	0.1657	0.7339	0.5682	0.02	16 879	4.46	649.51	$2.9021\text{E} + 03$

TABLE 2
Results of orthogonal estimator for data set 1

Term	Estimate	E	σ_{est}
$y(k-1)$	1.55930	0.98545	0.09079
$y(k-2)$	-0.44738	0.01351	0.16114
$y(k-3)$	-0.15585	0.60027×10^{-4}	0.07719
$u(k-1)$	1.28290	0.72154×10^{-5}	0.16776
$u(k-3)$	-1.19570	0.18119×10^{-3}	0.16177
$u(k-3)u(k-3)u(k-3)$	4.82620	0.38678×10^{-5}	2.39740
$0.2630e(k-3) - 0.2612e(k-4) - 0.239e(k-2) - 0.1618e(k-6) - 0.0461e(k-7) + 0.0469e(k-9)$ $- 0.031e(k-8) + 0.025e(k-5) - 0.001e(k-10) + 0.00062e(k-1)$			

TABLE 3
Results of orthogonal estimator for data set 2

Term	Estimate	E	σ_{est}
$y(k-1)$	1.54590	0.98269	0.08169
$y(k-2)$	-0.45829	0.01600	0.14191
$y(k-3)$	-0.13742	0.31174×10^{-4}	0.06787
$u(k-1)$	1.40430	0.21535×10^{-4}	0.17364
$u(k-3)$	-1.30990	0.21617×10^{-3}	0.16841
$u(k-3)u(k-3)u(k-3)$	5.88510	0.41526×10^{-4}	1.20810
$-0.2805e(k-2) - 0.171e(k-4) + 0.152e(k-3) - 0.1186e(k-6) + 0.031e(k-7) + 0.067e(k-1)$ $- 0.028e(k-8) + 0.0128e(k-10) - 0.016e(k-5) - 0.003e(k-9)$			

TABLE 4
Results of orthogonal estimator for data set 3

Term	Estimate	E	σ_{est}
$y(k-1)$	1.02800	0.98606	0.08449
$y(k-4)$	-0.43382	0.012410	0.070410
$y(k-2)$	0.05820	0.71540×10^{-4}	0.12640
$y(k-3)$	0.27386	0.29857×10^{-4}	0.11942
$u(k-1)$	1.82410	0.19159×10^{-4}	0.16255
$u(k-3)$	-1.71710	0.15014×10^{-3}	0.15756
$u(k-3)u(k-3)u(k-3)$	12.05900	0.42011×10^{-4}	1.86960
$+0.514e(k-1) - 0.138e(k-2) - 0.204e(k-6) - 0.198e(k-4) + 0.148e(k-5) - 0.120e(k-7)$ $- 0.099e(k-8) - 0.073e(k-9) - 0.062e(k-3) + 0.042e(k-10)$			

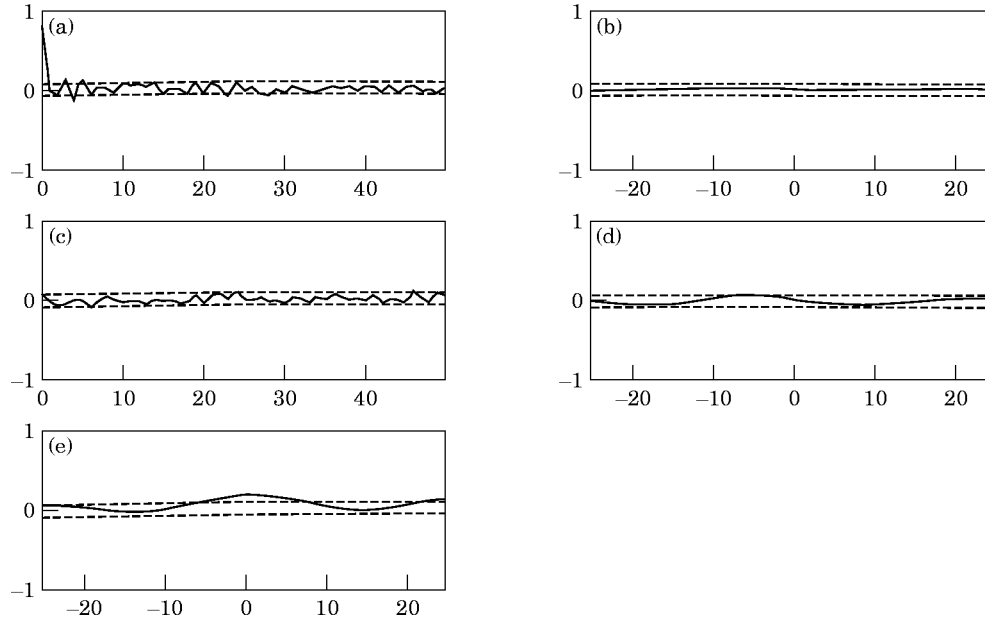


Figure 1. Correlation tests of the NARMAX model of a fixed cylinder for data set 1. (a) $\Phi_{(\epsilon_1 \epsilon_1)}$, (b) $\Phi_{(u_1 \epsilon_1)}$, (c) $\Phi_{(\epsilon_1 u_1)}$, (d) $\Phi_{(u_1 u_1)(\epsilon_1)}$, (e) $\Phi_{(u_1 u_1)(\epsilon_1 \epsilon_1)}$.

6. MODELLING OF SMALL-SCALE WAVE FORCE DATA

The velocity and force time histories for 22 different rectangular wave spectra with a fixed cylinder were obtained from the University of Salford [25]. The cylinder was subjected to random waves with rectangular spectral density functions having different bandwidths. The force was measured on a small cylindrical element and the input velocity is the ambient horizontal water particle velocity at the mid point of the element (obtained without the cylinder in position). These data were sampled with an uncertainty of 40 μ s. All wave tests had a variance of water surface elevation of 650 mm². The flow conditions were described by three parameters: KC, the Keulegan–Carpenter number (defined in the present study as $\sqrt{(2)u_{rms}T_w/D}$); Re, the Reynolds number $\sqrt{(2)u_{rms}D/\nu}$; and β , the Stokes number defined as $D^2/T_w\nu$. u_{rms} is the root mean square (rms) value of the horizontal velocity, T_w is the period associated with the peak in the velocity spectrum, and ν is the kinematic viscosity of fluid. The diameter and length of the cylindrical element are 0.038 m and 0.05067 m. Relevant information about the data sets used in the present study is shown in Table 1. Further details about the experimental set-up can be found in [25].

6.1. DISCRETE TIME MODELLING

Models were fitted between the in-line force and the horizontal water particle velocity. The input–output data were decimated by a factor of 2 (effective sampling frequency of 25 Hz) using the decimate function available in MATLAB [26]. This function filters the data with an eighth-order Chebyshev Filter that is basically a low-pass filter with a cut-off frequency equal to

$$f_{cutoff} = \frac{0.8 * f_s}{2R} \quad (44)$$

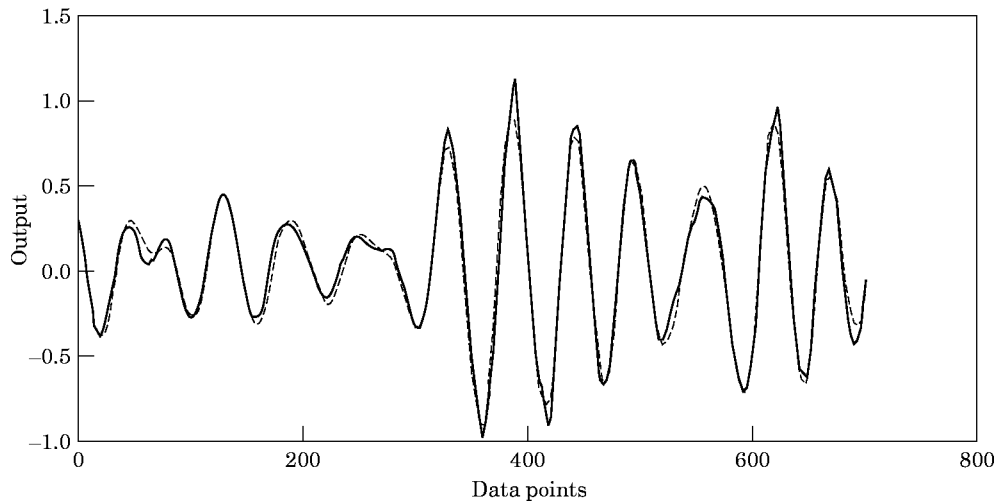


Figure 2. Model predicted output of the NARMAX model for the fixed cylinder for data set 1: estimation set. —, Model output; —, original output.

where f_s is the sampling frequency of the original data and R is the decimation factor. The original spectral information of the data is not lost due to decimation. The above sampling was chosen using the procedures described in Section 3.3. In order to fit a discrete NARMAX model, 700 data points were used for estimation purposes and the model validation was done with a sequence of 1000 points of input–output data taken arbitrarily from the rest of the available data points. The discrete NARMAX models were fitted to the data sets 1, 2 and 3 with an initial model specification of $n_u = 3$, $n_y = 3$, $n_d = 10$, and $N_l = 3$. The terms that were selected together with their associated parameter estimates, error reduction ratios (E) and the standard deviation of the parameters are tabulated in Tables 2–4. Note that from no a priori knowledge, the estimator selects the significant terms to include in the model and ranks them in the order given in Tables 2–4. Multiplying the E values by 100 gives the % contribution that each term makes to the variance of the

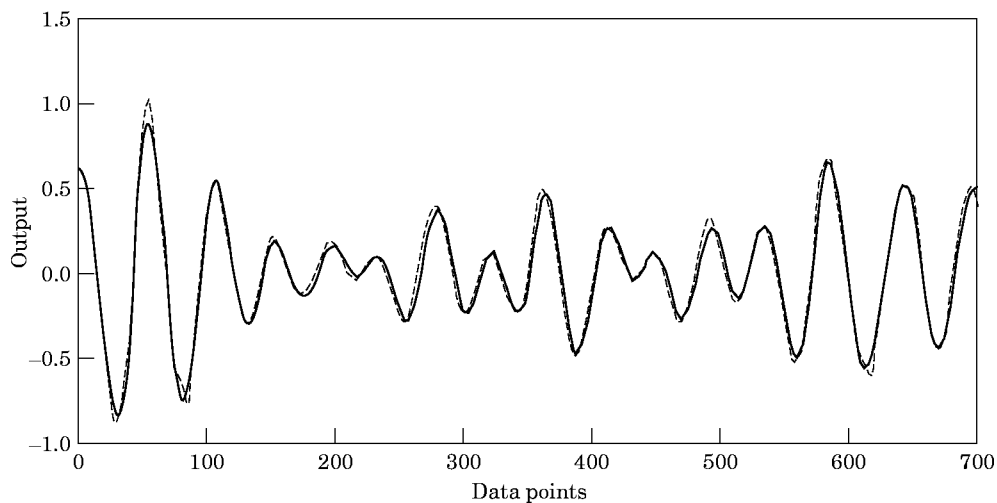


Figure 3. Model predicted output of the NARMAX model for the fixed cylinder for data set 1: test set. ---, Model output; —, original output.

TABLE 5
Normalised mean square errors of NARMAX models of Salford cylinder

Data set	NMSE of one-step-ahead output ($\times 10^{-4}$)	NMSE of model predicted output ($\times 10^{-2}$)
1	6.56	1.66
2	8.73	1.88
3	9.90	2.28

output. The estimated noise model is given in the last row of each table. Note that the estimation of noise model is essential to ensure that the parameters of the process model are unbiased.

The correlation plots and model predicted outputs over the estimation and test sets for data set 1 are shown in Figs 1–3. The respective plots for the models fitted to other data sets were quite satisfactory (data not shown), and the normalised mean squared errors based on the one-step-ahead predictions and model predicted outputs are shown in Table 5.

The results suggest the estimated NARMAX model for data set 1 is unbiased and the predictive performance of the model is excellent. The model generalises well over the rest of the data points [Fig. 1(c)], and may be used for predicting the wave forces for any set of input data.

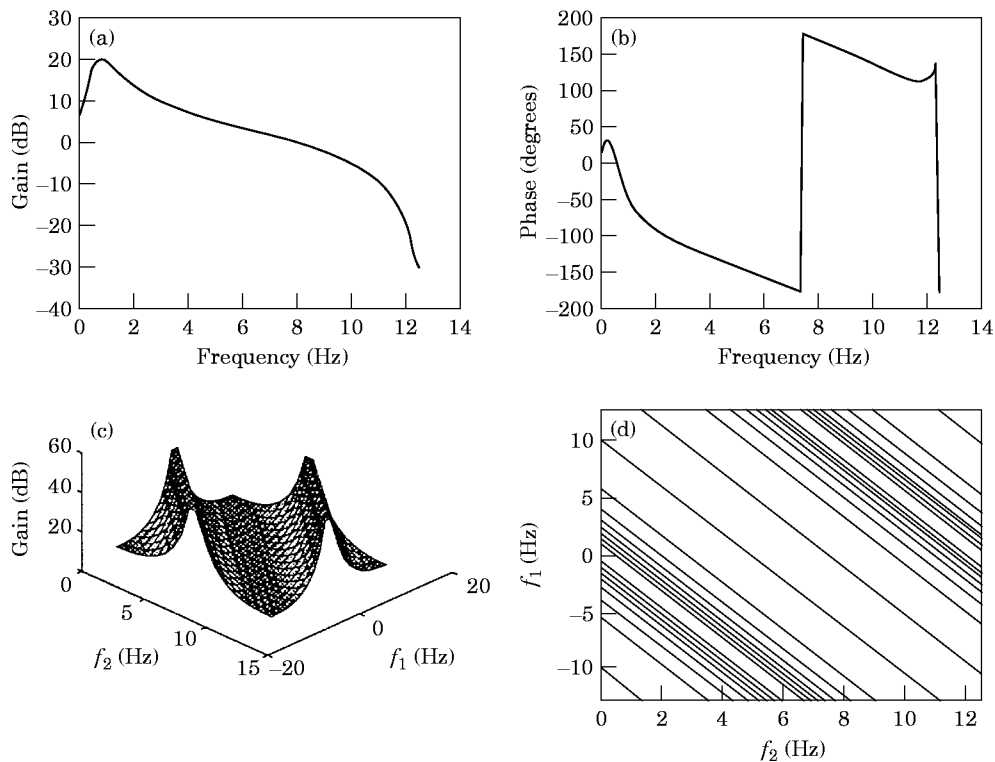


Figure 4. (a) Gain $H_1(f_1)$, (b) phase, (c) gain $H_3(f_1, f_2, f_3)$, and (d) gain contour for the NARMAX model of data set 1.

TABLE 6

Characteristics of the frequency response functions of NARMAX models of Salford cylinder

Data set	Resonant frequency (linear) (Hz)	Max, linear gain (dB)	Ridge equation ($f_1 + f_2 + f_3$)	Max, non-linear gain (dB)
1	0.825	20.1014	0.55	40.988
2	0.900	20.03	0.475	41.47
3	0.775	19.99	0.6	45.92

6.2. FREQUENCY DOMAIN ANALYSIS

The plots of the linear and third-order frequency response functions of the estimated discrete NARMAX model for data set 1 are shown in Fig. 4.

The magnitude plot of $H_1(f_1)$ shows a peak value of 20.10 dB at a frequency 0.825 Hz which corresponds to the linear resonant frequency and thereafter decreases monotonically. This is in contrast to the linear frequency response of the general form of the Morison model [equation (6)] which increases with frequency. Since the NARMAX model of the system does not contain any second-order non-linear terms, $H_2(f_1, f_2)$ is absent. From the gain plot of the third-order frequency response function, the peak magnitude of $H_3(\cdot)$ is found to be 40.98 dB. This compares with a maximum of the linear gain of 20.1 dB and shows that the system possesses a dominant non-linear characteristic. This occurs when the system is excited by an input whose frequency sum equals 0.55 Hz, that is when $f_1 + f_2 + f_3 = 0.55$ Hz, which corresponds to the ridge in the contour plot. This shows that there will a significant amount of energy shift to the lower frequency region under certain conditions of input excitation due to the non-linear effects. This cannot be explained from the Morison model where $H_3(\cdot)$ [equation (7)] will be a constant for all frequencies with no ridges. The information from the frequency response functions of the

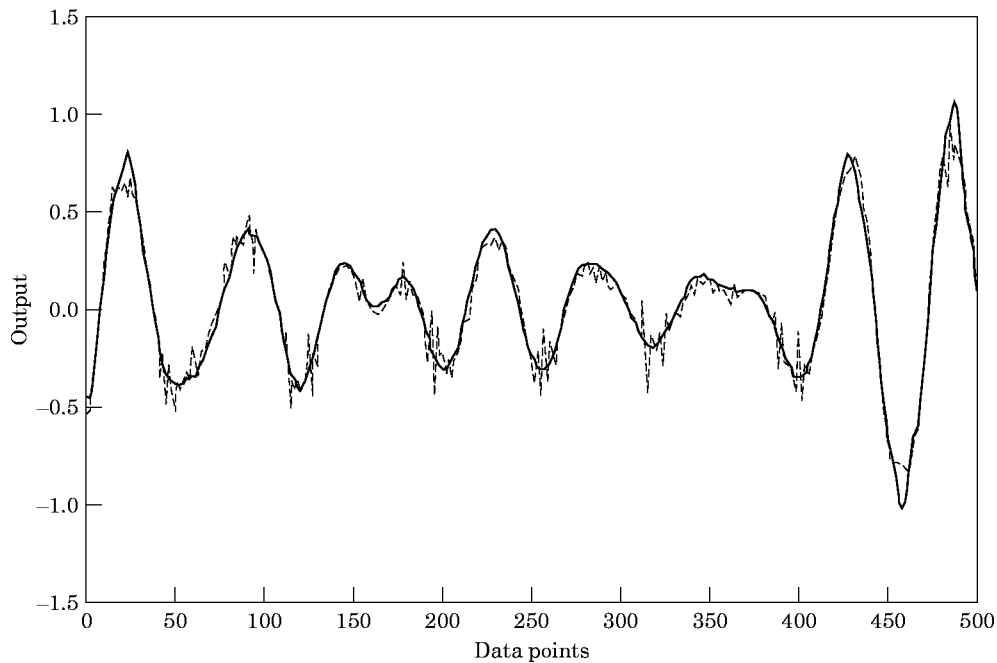


Figure 5. Morison fit for data set 1. —, Morison model output; —, original output.

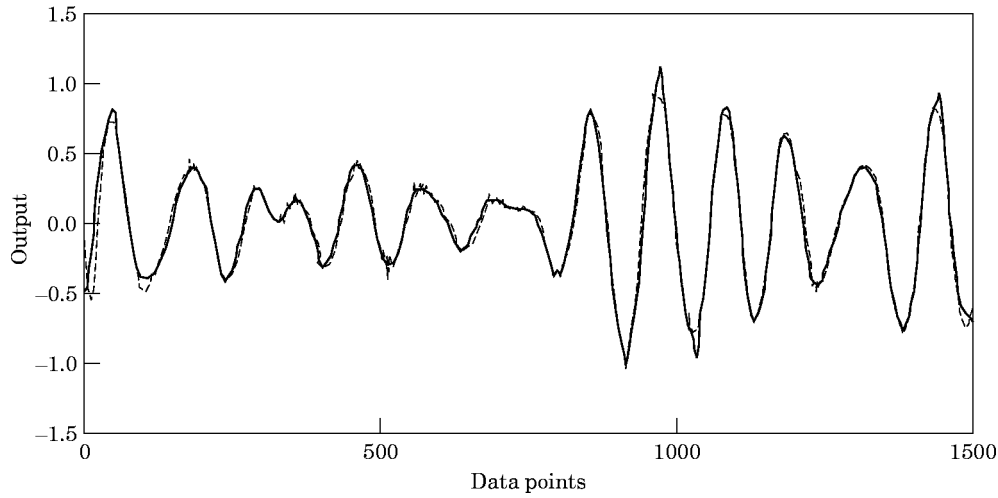


Figure 6. Response of the continuous time model for data set 1 of the Salford cylinder.

estimated models shown in Tables 3 and 4 is summarised in Table 6 and this shows a reasonable consistency over the data sets which represent excitation at different bandwidths.

6.3. ESTIMATION OF NON-LINEAR CONTINUOUS TIME MODELS

Having fitted discrete NARMAX models to the input–output data and computed the GFRF, the final step is to estimate continuous time non-linear differential equation models

TABLE 7
Normalised MSE of reconstructed models of the Salford cylinder

Data set	Normalised mean square error
1	0.0339
2	0.0427
3	0.0656

TABLE 8
Results of orthogonal estimation for Christchurch Bay Data

Term	Estimate	E	σ_{est}
$y(k-1)$	2.32430	0.95596	0.16485
$y(k-2)$	-1.95280	0.02957	0.28459
$y(k-3)$	0.56292	0.33298×10^{-3}	0.13803
$u(k-2)$	-55.95300	0.16349×10^{-4}	14.68800
$u(k-1)$	57.43400	0.00148	15.30400
$u(k-1)u(k-1)u(k-1)$	1.51840	0.19230×10^{-3}	0.71450

$+0.1478e(k-6) + 0.107e(k-15) - 0.0457e(k-3) - 0.097e(k-18)$
 $-0.568e(k-1) + 0.164e(k-4) + 0.054e(k-17) + 0.063e(k-20)$
 $+0.0638e(k-5) + 0.0505e(k-9) - 0.068e(k-16) - 0.044e(k-13)$
 $-0.036e(k-7) + 0.0395e(k-2) - 0.026e(k-12)$

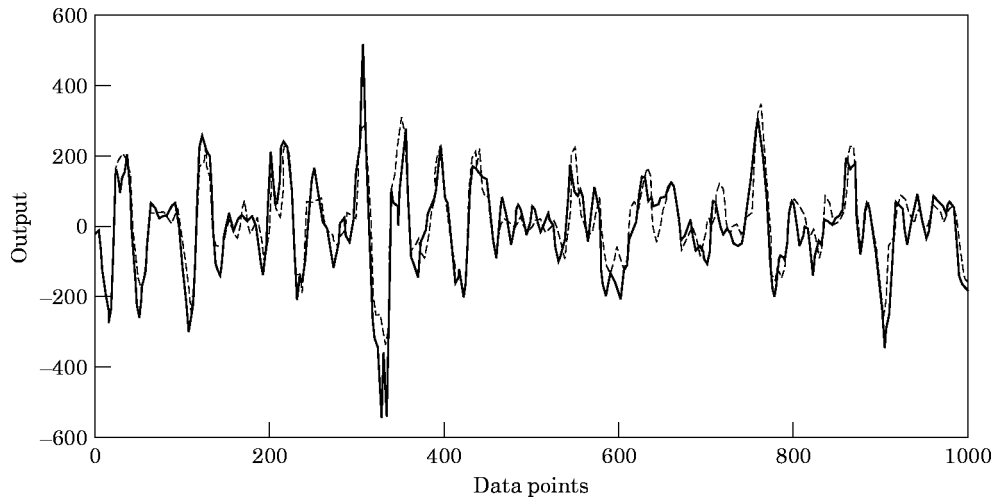


Figure 7. Model predicted output of NARMAX model of the Christchurch Bay data. —, Model output; —, original output.

by curve fitting to the GFRF. Note that the accuracy of the final estimated continuous time model depends on the accuracy of the discrete model. Hence it is appropriate to make a comparative analysis of the Morison model with the discrete NARMAX model prior to reconstructing non-linear continuous time models using the new approach.

6.3.1. Discrete NARMAX vs Morison model

The Morison equation fitted to the data set 1 using conventional least squares curve fitting is given by

$$y = 2.3264\dot{u} + 34.3064u|u|. \quad (45)$$

The approximated Morison equation fitted to the data is given by

$$y = 2.3264\dot{u} + 1.4192u + 175.90u^3. \quad (46)$$

The Morison equation appears to fit the data quite well (Fig. 5). When estimating the parameters of a given model from a set of input–output data, however, it is essential to investigate whether the model has successfully captured the system dynamics. This is very important if the models are to yield good predictions of the system output for different input excitations and is not simply a curve fit to one data set. It is simple to show that the linear transfer function of the Morison model increases monotonically as the frequency increases thus exhibiting high-frequency instability which is not expected from the original input–output data. The Morison models fitted to the other data sets have similar behaviour to the present model (see later).

TABLE 9

Normalised mean square error of NARMAX models of Christchurch Bay

Model	NMSE of one-step-ahead output	NMSE of model predicted output
Christchurch Bay	0.0114	0.2433

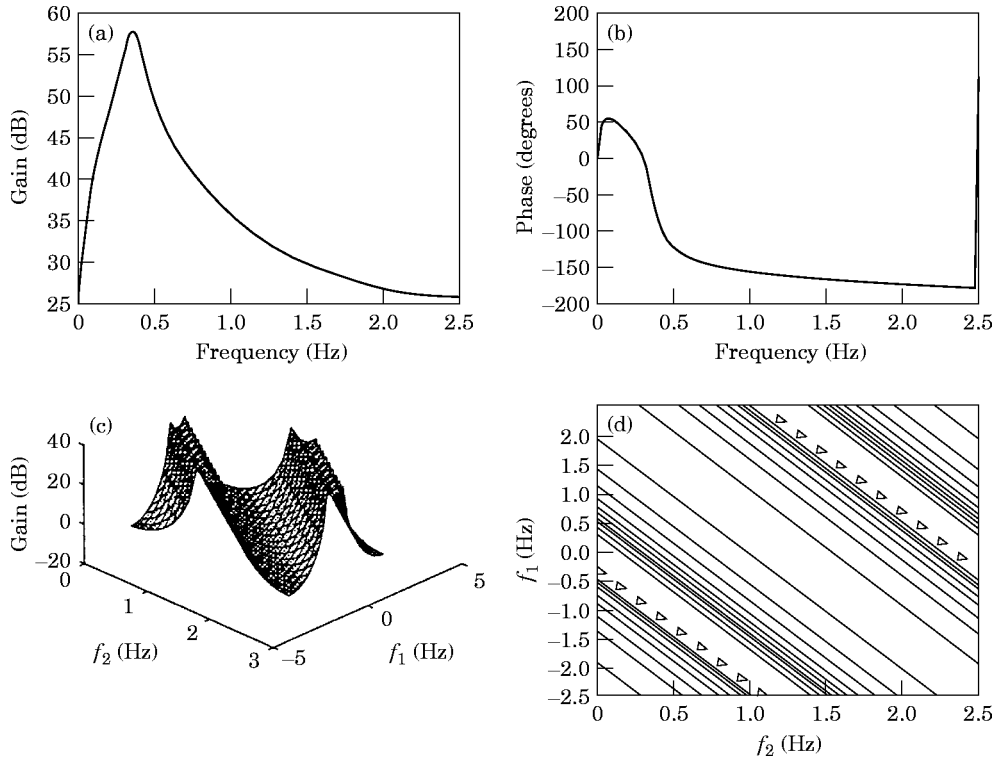


Figure 8. (a) Gain $H_1(f_1)$, (b) phase, (c) gain $H_3(f_1, f_2, f_3)$, and (d) gain contour for the NARMAX model of the Christchurch Bay data.

6.3.2. Reconstruction of the non-linear continuous time model

It has been shown that the NARMAX model explains the dynamics in the data much better than the Morison model. However, the parameters of the NARMAX model cannot be interpreted easily. In the present search for a possible extension of the Morison equation, and to have a physically interpretable model, a non-linear continuous time model needs to be estimated. This is done by curve fitting to the GFRF computed from the NARMAX model.

The discrete NARMAX model fitted to data set 1 (Table 2) is given by

$$\begin{aligned}
 y(k) = & 1.5593y(k-1) - 0.44738y(k-2) \\
 & - 0.15585y(k-3) + 1.2829u(k-1) \\
 & - 1.195u(k-1) + 4.8262u(k-3)u(k-3)u(k-3) \\
 & + \Theta_\xi.
 \end{aligned} \tag{47}$$

The last term in equation (47) corresponds to the noise terms in Table 2.

In order to reconstruct the linear part of the continuous time system, 100 equally spaced frequency response data were generated in the frequency range 0–5 Hz and the weighting parameter λ was chosen to be 4.0. For the reconstruction of the non-linear third-order part, 64 equally spaced frequency response data were generated in the frequency range 0–0.2 Hz. It was found that with the inclusion of a u^3 term, the sum of the error reduction ratio (E)

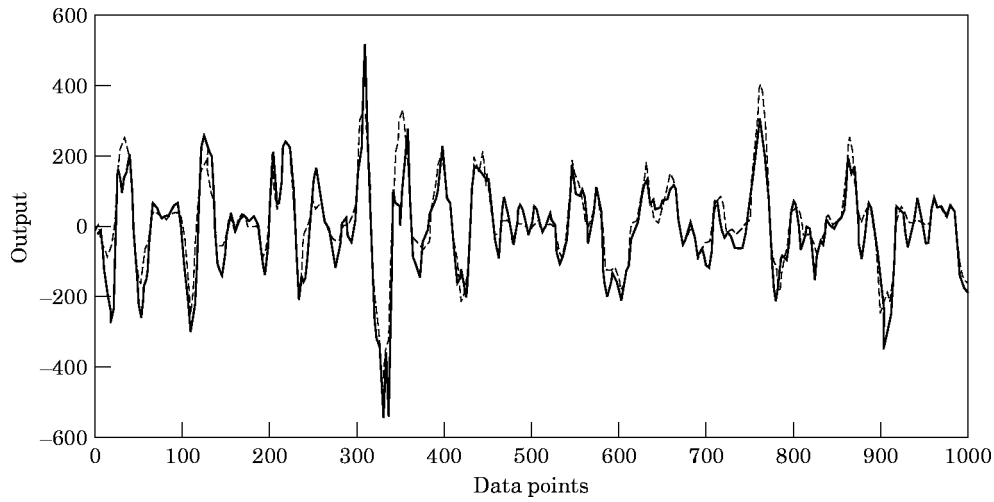


Figure 9. Response of the Morison model for the Christchurch Bay data. —, Morison model; — —, original output.

values equaled 99.77%, which means that this term is adequate to capture almost all of the non-linear dynamics of the system. The final model was given by

$$0.00145 \frac{d^3 y}{dt^3} + 0.0463 \frac{d^2 y}{dt^2} + 0.2609 \frac{dy}{dt} + y = 2.2701 \frac{du}{dt} + 1.983u + 109.855u^3. \quad (48)$$

To validate further the reconstructed continuous time model, the output response of the model in equation (47) was compared with the original data (Fig. 6). It is clear that the estimated continuous time model performs well in predicting the output force. Continuous time models were also reconstructed for the models of data sets 2 and 3 under identical conditions. The normalised mean square errors of the reconstructed models were compared with the actual output (Table 7).

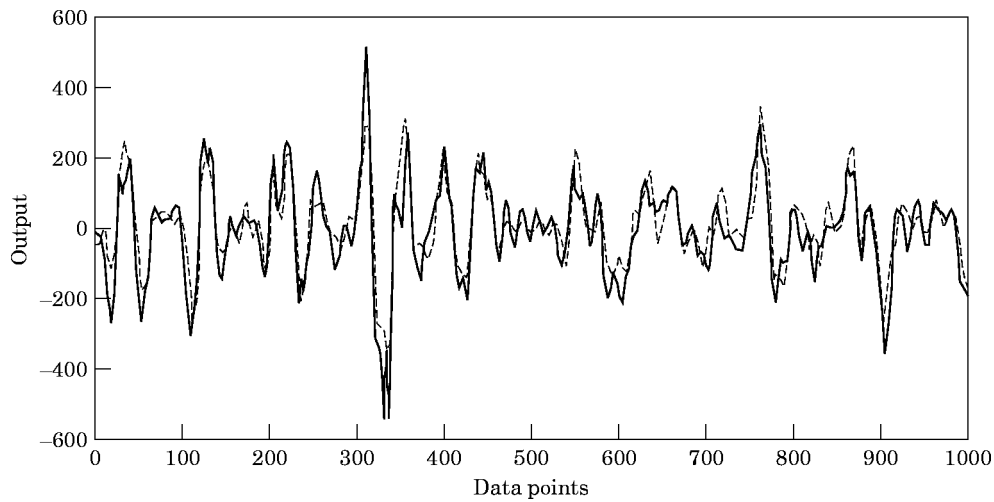


Figure 10. Response of the continuous time model for the Christchurch Bay data. —, Continuous model; — —, original output.

TABLE 10

Results of orthogonal estimator for the De Voorst tube

Terms	Estimate	E	σ_{est}
$y(k-1)$	0.84684	0.99322	0.36790
$y(k-3)$	-0.41859	0.00317	0.03304
$u(k-4)$	-0.23755×10^3	0.28243×10^{-3}	50.80600
$u(k-1)$	0.29322×10^3	0.33148×10^{-3}	82.54500
$y(k-2)$	0.35113	0.92201×10^{-4}	0.046966
$u(k-4)u(k-4)u(k-4)$	16.42600	0.71055×10^{-4}	2.43740
$u(k-2)$	-57.09300	0.16406×10^{-4}	0.12668×10^{-3}

7. MODELLING OF WAVE FORCE DATA FROM A DIRECTIONAL SEA STATE

In this section, the new model structures are fitted to forces and velocities measured on the 0.48-m diameter column of the Christchurch Bay Tower described by Bishop [2]. The sea has wave heights of 7 m and is directional with a prominent current. The forces were measured on a section of column 0.535 m long and the velocities were measured with calibrated perforated ball meters attached at a distance of 1.228 m from the cylinder axis. This will not give the exact velocity at the centre of the force sleeve unless waves are unidirectional with crests parallel to the line joining the velocity meter to the cylinder. This is called the y direction and the normal to this is the x direction. The waves, however, always vary in direction, so in order to facilitate the fitting of a single-input single-output (SISO) model, the data was chosen from an interval when the oscillatory velocity in the x direction was large and that in the y direction small. The KC , Re and β values of the data are 20.56, 5.21×10^5 and 2.53×10^4 , respectively.

To fit a discrete NARMAX model, all the available 1000 data points were used for estimation. The model was fitted to the input-output data with an initial model specification of $N_f = 3$, $n_u = 2$, $n_y = 3$, and $n_e = 20$ (for more details, see Table 8).

From the results, it is found that the fitted NARMAX models provided acceptable predictive performance, (Fig. 7 and Table 9).

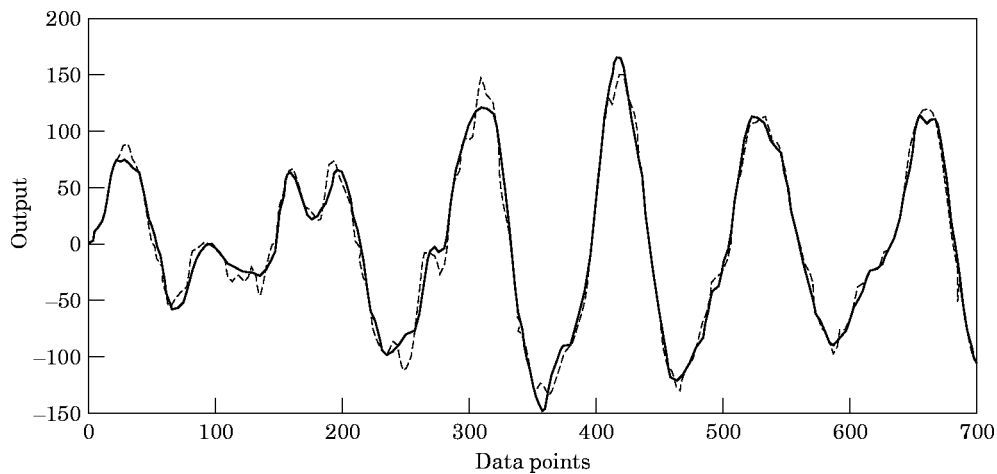


Figure 11. Model predicted output of the NARMAX model of the De Voorst tube: estimation set. ---, Model output; —, original output.

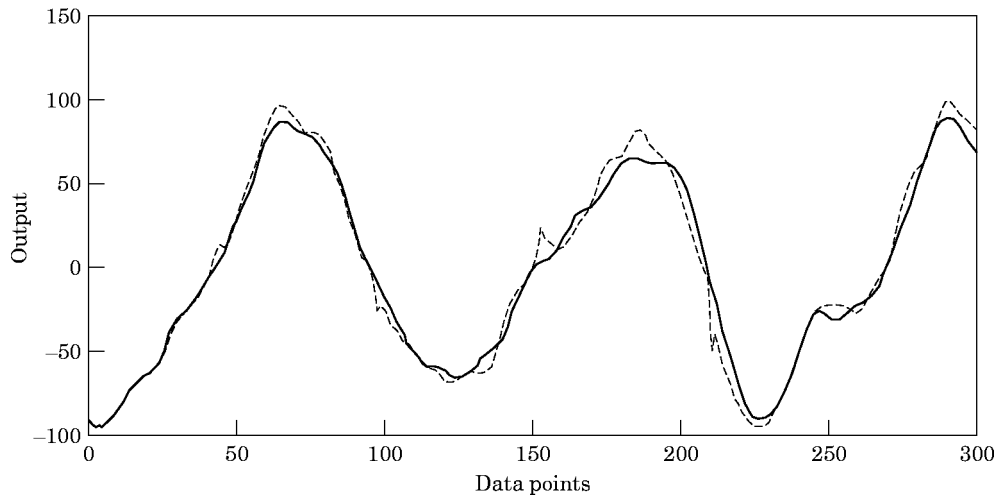


Figure 12. Model predicted output of the NARMAX model of the De Voorst tube: test set. ---, Model output; —, original output.

7.1. FREQUENCY DOMAIN ANALYSIS

The magnitude of the higher-order frequency response function shows that there is a significant non-linear effect (Fig. 8). The plot of the linear frequency response function shows that the linear resonant frequency of the system is 0.3535 Hz with a magnitude of 57 dB and that is followed by a decreasing trend as the frequency is increased. This type of characteristic cannot be provided by the Morison model. From the third-order frequency response plot, the maximum magnitude of $H_3(\cdot)$ is around 40 dB indicating that the non-linear effects of the system are significant. The non-linear ridges occur due to the interaction among input frequency components whose frequency sums equal 0.375 and 0.35 Hz.

7.2. ESTIMATION OF NON-LINEAR CONTINUOUS TIME MODEL OF CHRISTCHURCH BAY MODEL

Before estimating the non-linear continuous time models from the GFRF, a Morison equation model was fitted to the data using least squares to yield

$$y(t) = 148.6776\dot{u} + 90.5731u|u|. \quad (49)$$

The continuous time Morison equation with cubic approximation of the function $u|u|$ is given by

$$y(t) = 148.6776\dot{u} + 54.339u + 32.02u^3. \quad (50)$$

The response of the Morison equation was compared with the original data and shows a reasonably good fit (Fig. 9).

TABLE 11

Normalised mean square error of NARMAX models of the De Voorst tube data

Model	NMSE of one-step-ahead output	NMSE of model predicted output
De Voorst tube	0.0023	0.0192

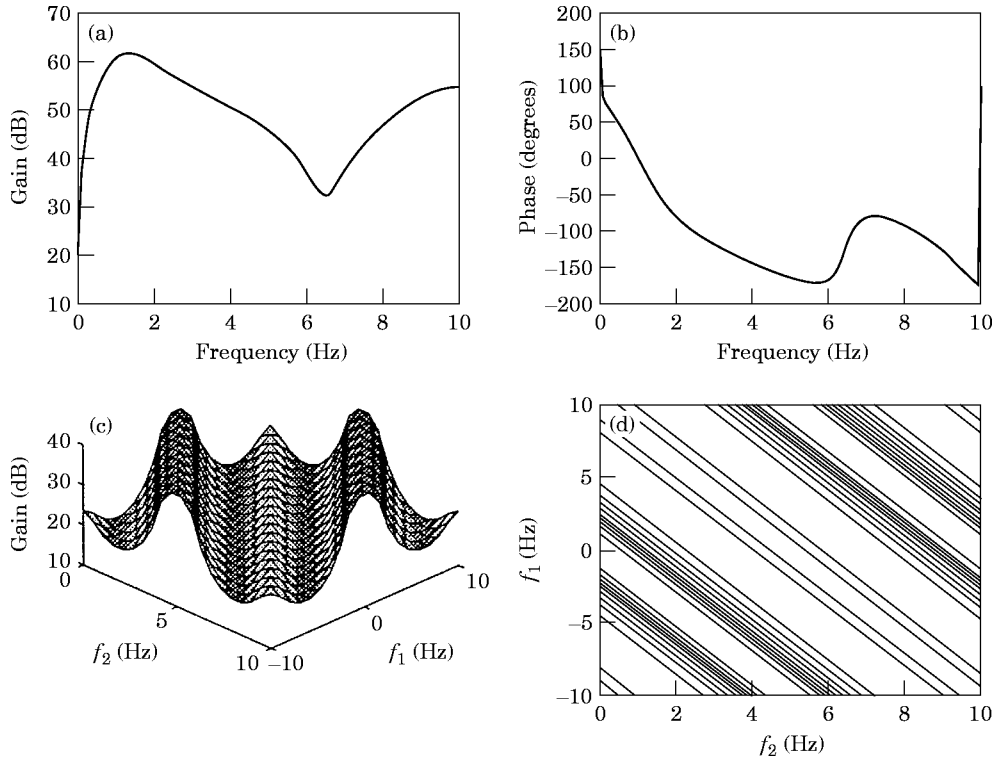


Figure 13. (a) Gain $H_1(f_1)$, (b) phase, (c) gain $H_3(f_1, f_2, f_3)$, and (d) gain contour for the NARMAX model of the De Voorst tube model.

It is simple to show that the Morison model is simply a curve fit to the data and does not represent correctly the underlying dynamics in the data. The third-order transfer function $H_3(\cdot)$ of the Morison model has a magnitude of 30.10 dB and remains constant at all frequencies and does not possess any ridges compared to the third-order transfer function of Fig. 8(c).

7.3. RECONSTRUCTION OF CONTINUOUS TIME MODELS

The discrete NARMAX model of the system is given by

$$\begin{aligned}
 y(k) = & 2.3243y(k-1) - 1.9528y(k-2) + 0.5629y(k-3) \\
 & - 55.9534u(k-2) + 57.4343u(k-1) + 1.5184u(k-1)u(k-1)u(k-1) \\
 & + \Theta_\xi.
 \end{aligned} \quad (51)$$

In order to reconstruct the linear part of the continuous time system, 100 equally spaced frequency response data were generated in the frequency range 0–2.5 Hz and the weighting parameter λ was fixed at 10. For the reconstruction of the non-linear part, 64 equally spaced third-order frequency response data were generated in the frequency range 0–0.1 Hz. It was found that with the inclusion of the term u^3 , the sum of the E values equalled 99.1% which suggests that this term is adequate to capture the non-linear dynamics of the system. The resulting continuous time model was given by

$$0.089 \frac{d^3 y}{dt^3} + 0.2581 \frac{d^2 y}{dt^2} + 0.6101 \frac{dy}{dt} + y = 178.69 \frac{du}{dt} + 33.6343u + 23.1578u^3. \quad (52)$$

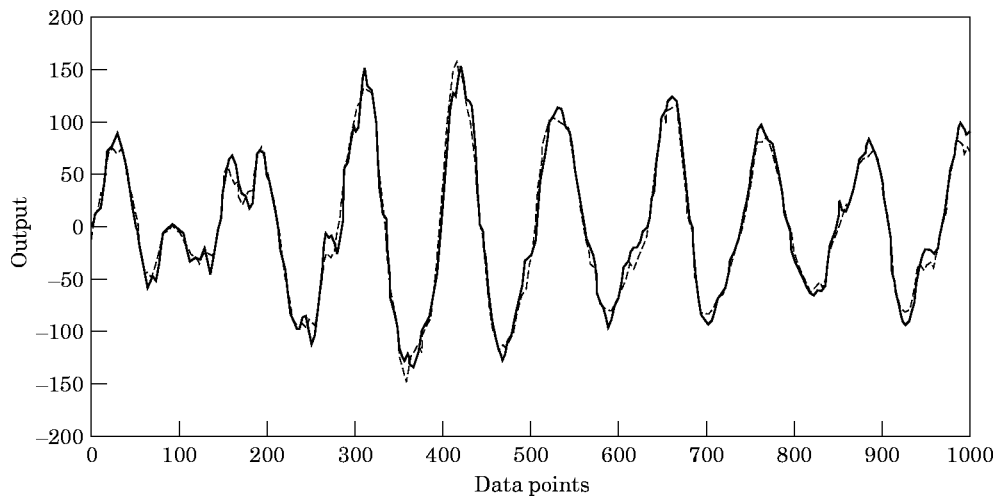


Figure 14. Response of the Morison model of the De Voorst tube data ---, Morison model; —, original output.

The response of the continuous time model is shown in Fig. 10, and the normalised mean square error between the actual output and the output of the reconstructed continuous time system for the Christchurch Bay model was 0.2562.

8. MODELLING OF WAVE FORCE DATA FROM DE VOORST

This data set was obtained from the delta flume of the De Voorst facility at Delft Hydraulics. The particular data considered here come from run OA1F1 which used a fixed smooth cylinder. The same cylinder was used as in Christchurch Bay but the sea states have smaller wave heights (up to 2 m, compared to 7 m at Christchurch Bay). The unidirectional wave profiles were generated so that the surface elevation spectrum approximated to a JONSWAP spectrum. More details of the experiment can be found in

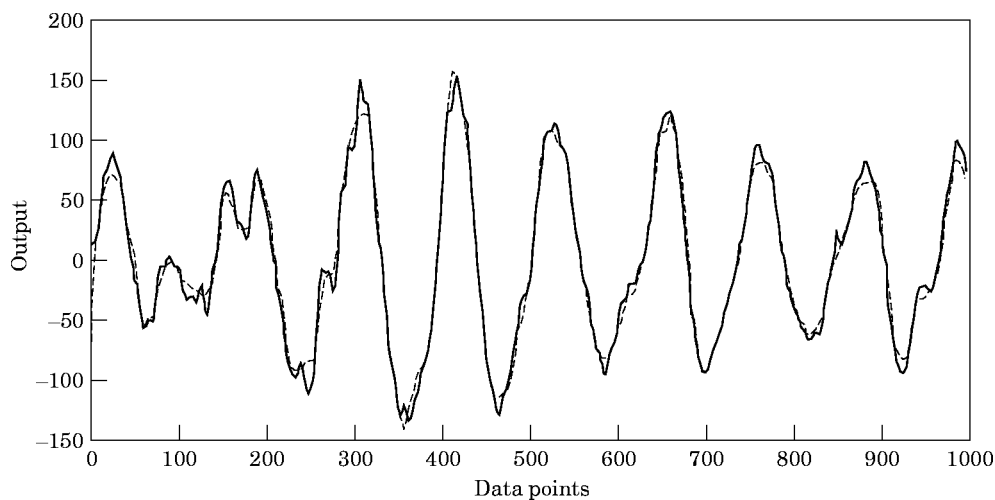


Figure 15. Response of the continuous time model. ---, Continuous model; —, original output.

TABLE 12
Continuous time models for data set 1

	Model	C_m	C_d	NMSE
Morison	$y = 2.3264 \frac{du}{dt} + 34.3064u u $	2.0500	1.8056	0.0394
Reconstructed (NARMAX)	$0.00145 \frac{d^3y}{dt^3} + 0.0463 \frac{d^2y}{dt^2} + 0.2609 \frac{dy}{dt} + y =$ $2.2701 \frac{du}{dt} + 1.983u + 109.855u^3$	2.0000	1.7573	0.0339
Dynamic Morison (reconstructed)	$0.04564 \frac{d^2y}{dt^2} + 0.2229 \frac{dy}{dt} + y =$ $2.1485 \frac{du}{dt} + 2.094u + 108.1211u^3$	1.8936	1.8178	0.0322
Dynamic Morison (without history term)	$y = 2.1485 \frac{du}{dt} + 2.094u + 108.1211u^3$	1.8936	1.8178	0.0621

Davies *et al.* [28] which contains an exhaustive wave-by-wave Morison analysis of the full De Voorst data set. In the experiment, the horizontal velocity was obtained from electromagnetic flowmeters placed adjacent to the cylinder at the same distance from the wave maker. The forces were recorded from force sleeves placed at three levels (stations 2, 3 and 4) on the cylinder. The data from station 2 was discarded as the sleeve fell within the crest to trough region of the wave. Of those remaining, station 3 was nearest to the surface while fully immersed and was consequently subjected to the highest non-linear forces. For this reason, data from station 3 are used in the following analysis. The KC, β and Re values of the flow are 5.8030, 4.14×10^4 and 2.40×10^5 , respectively.

Out of several thousand input-output pairs of the OA1F1 data set, the most non-linear data were taken for model estimation. It is known that for the successful identification of any system the input should be persistently exciting so as to excite all the relevant modes

TABLE 13
Continuous time models for data set 2

	Model	C_m	C_d	NMSE
Morison	$y = 2.1243 \frac{du}{dt} + 35.70u u $	1.8715	1.8789	0.0487
Reconstructed (NARMAX)	$0.0012 \frac{d^3y}{dt^3} + 0.04067 \frac{d^2y}{dt^2} + 0.2556 \frac{dy}{dt} + y =$ $2.191 \frac{du}{dt} + 1.894u + 118.113u^3$	1.9311	1.7076	0.0427
Dynamic Morison (reconstructed)	$0.04029 \frac{d^2y}{dt^2} + 0.22057 \frac{dy}{dt} + y =$ $2.086 \frac{du}{dt} + 1.992u + 116.441u^3$	1.8385	1.7537	0.0422
Dynamic Morison (without history term)	$y = 2.086 \frac{du}{dt} + 1.992u + 116.441u^3$	1.8385	1.7537	0.0467

TABLE 14
Continuous time models for data set 3

	Model	C_m	C_d	NMSE
Morison	$y = 2.1435 \frac{du}{dt} + 33.9967u u $	1.8892	1.7893	0.0614
Reconstructed (NARMAX)	$0.000484 \frac{d^3y}{dt^3} + 0.04729 \frac{d^2y}{dt^2} + 0.2061 \frac{dy}{dt} + y =$ $1.9302 \frac{du}{dt} + 1.450u + 163.545u^3$	1.7012	1.7188	0.0656
Dynamic Morison (reconstructed)	$0.04698 \frac{d^2y}{dt^2} + 0.19334 \frac{dy}{dt} + y =$ $1.9001 \frac{du}{dt} + 1.4979u + 162.322u^3$	1.6746	1.7367	0.0452
Dynamic Morison (without history term)	$y = 1.90001 \frac{du}{dt} + 1.4979u + 162.322u^3$	1.6746	1.7367	0.0726

(both linear and non-linear) of the system. In the present example, this corresponds to the case where the velocity is high. Since one useful sign of non-linearity is the size of the transverse component of the force which is caused entirely by vortex shedding, the data for analysis were chosen to be centred about the instant of maximum transverse force excursion.

The model of the De Voort tube data was estimated based on the data sampled at 20 Hz. In order to fit a discrete NARMAX model, 700 data points were used for estimation and the remaining 300 data points were used for model validation. The model estimated with an initial specification of $N_l = 3$, $n_y = 5$, $n_u = 4$ and $n_e = 20$ with proper model validation is given in Table 10.

TABLE 15
Summary of results for christchurch bay data

	Model	C_m	C_d	NMSE
Morison	$y = 148.6776 \frac{du}{dt} + 90.5731u u $	1.5351	0.7054	0.2145
Reconstructed (NARMAX)	$0.089 \frac{d^3y}{dt^3} + 0.2581 \frac{d^2y}{dt^2} + 0.6101 \frac{dy}{dt} + y =$ $178.69 \frac{du}{dt} + 33.6343u + 23.1578u^3$	1.8450	0.4621	0.2562
Dynamic Morison (reconstructed)	$0.2791 \frac{d^2y}{dt^2} + 0.563 \frac{dy}{dt} + y =$ $171.145 \frac{du}{dt} + 23.00u + 23.25u^3$	1.7671	0.4037	0.2596
Dynamic Morison (without history term)	$y = 171.145 \frac{du}{dt} + 23.00u + 23.25u^3$	1.7671	0.4037	0.3084

TABLE 16
Summary of results for de Voorst tube data

	Model	C_m	C_d	NMSE
Morison	$y = 169.666 \frac{du}{dt} + 95.9804u u $	1.7518	0.7475	0.0233
Dynamic Morison (reconstructed)	$0.02236 \frac{d^2y}{dt^2} + 0.1606 \frac{dy}{dt} + y =$ $171.94 \frac{du}{dt} + 4.8118u + 74.0056u^3$	1.7753	0.4120	0.0584
Dynamic Morison (without history term)	$y = 171.94 \frac{du}{dt} + 4.8118u + 74.0056u^3$	1.7753	0.4120	0.0404

The model predicted output and the model validated outputs are shown in Figs 11 and 12. The normalised mean square errors based on one-step-ahead prediction and model predicted outputs are shown in Table 11.

8.1. FREQUENCY DOMAIN ANALYSIS

From the linear frequency response plots it is evident that the magnitude of $H_1(\cdot)$ reaches a maximum value of around 60 dB (Fig. 13). It does not show a continually increasing trend. The magnitude of the higher-order frequency response function shows that there is a significant non-linear effect [represented by the ridges in Fig. 13(c)] which occur when the sum of the frequencies of the input excitation equals 0.4 Hz.

8.2. DISCRETE NARMAX VS MORISON MODEL

The Morison model estimated from the data by least squares is given by

$$y(t) = 169.666\dot{u} + 95.9804u|u|. \quad (53)$$

The continuous time Morison equation with cubic approximation of the function $u|u|$ is given by

$$y(t) = 169.666\dot{u} + 27.054u + 72.22u^3. \quad (54)$$

The response of the Morison equation is compared with the original data in Fig. 14. The magnitude of third-order transfer function, $H_3(\cdot)$, is 37.17 dB which remains constant for all frequencies.

TABLE 17
Summary of results

Model	T_w	γ_0	γ_1	C_m	C_d	KC	Re
Data set 1	2.164	0.90	0.103	1.89	1.82	4.74	3.16×10^3
Data set 2	2.2109	0.83	0.0997	1.84	1.75	4.95	3.23×10^3
Data set 3	2.2232	1.26	0.0869	1.67	1.74	4.46	2.90×10^3
Christchurch Bay	9.090	0.88	0.062	1.77	0.40	20.5	5.21×10^5
De Voorst Tube	5.5555	0.87	0.0289	1.77	0.41	5.80	2.4×10^5

8.3. RECONSTRUCTION OF THE CONTINUOUS TIME MODEL

From Table 11, the discrete NARMAX model is given by

$$\begin{aligned} y(k) = & +0.84684y(k-1) - 0.41859y(k-3) \\ & - 237.55u(k-4) + 293.22u(k-1) \\ & + 16.426u(k-4)u(k-4)u(k-4) - 57.09u(k-2) + \Theta_{\xi}. \end{aligned} \quad (55)$$

The linear part of the continuous time model was reconstructed by generating 100 equally spaced frequency response data in the frequency range 0–2.5 Hz and the weighting parameter λ was fixed at 5.0. For the reconstruction of the non-linear part, 64 equally spaced frequency response data in the frequency range 0–0.04 Hz were used. It was found that with the selection of the u^3 term, the sum of the error reduction ratios became 96% and the contribution of other terms in subsequent iterations was found to be negligible. This implies that the system has a dominant third-order non-linearity in the input. The estimated continuous time model was given by

$$0.02236 \frac{d^2y}{dt^2} + 0.1606 \frac{dy}{dt} + y = 171.94 \frac{du}{dt} + 4.8118u + 74.0056u^3. \quad (56)$$

The output response of the continuous time model is compared with the original in Fig. 15. The normalised mean squared errors between the actual output and the output of the reconstructed continuous time system for the De Voorst time data was 0.0584.

9. A PROPOSED EQUATION STRUCTURE

9.1. STRUCTURAL CHARACTERISTICS OF MORISON'S EQUATION

In the simulated examples based on experimental data, it has been observed that the Morison equation fits the data reasonably well but fails to capture the underlying system dynamics. Equation (4) shows that the Morison equation is essentially an infinite-order polynomial in the input with an additional term consisting of the input derivative that partly takes into account the inviscid effect of flow acceleration. The Morison equation is therefore a polynomial approximation to a system and the well-known limitations of polynomial curve fitting apply. A polynomial of too low an order cannot capture the structure in the data whereas a polynomial of too high an order will tend to overfit and have poor generalisation properties.

Although the wake flows that generate forces in waves are complex and so an accurate representation is often difficult to achieve, it can be shown that the wave force at any particular instant depends on the flow acceleration, the rate of vorticity shed and the flow behaviour in the recent past [29]. The Morison model can capture the first two effects due to the presence of the input derivative and the drag term, but has failed to represent the effects of flow behaviour in the past because of the absence of any output dynamics.

An extended version of the Morison equation called the Morison–Duffing equation has been proposed by Stansby *et al.* [4] to provide a better fit than the Morison equation to data collected from several flow situations. The Morison–Duffing equation is given by

$$\alpha_3 \ddot{F} + \alpha_2 \dot{F} + \alpha_1 F|F| + F = 0.5\rho DC_d u|u| + 0.25\pi\rho D^2 C_m \dot{u}. \quad (57)$$

The higher-order derivative terms of the force are included to represent the history effects, and the term $F|F|$ has been included to represent other effects of non-linearity and improve the fit. However, it may be shown that since the drag term $u|u|$ is a polynomial of infinite

order, it can emulate all the higher-order non-linear effects which can be represented by the output drag term $F|F|$. Hence the $F|F|$ drag term in the Morison–Duffing equation is not necessary in an equation correctly modelling the dynamic structure which is achieved below.

9.2. DYNAMIC MORISON EQUATION

The results of fitting non-linear continuous time differential equation models to data for a variety of flow situations have been given in Sections 6–8. Although in the estimation process no a priori assumptions have been made regarding the structure of the models, both during the estimation of the discrete NARMAX model or during the reconstruction of continuous time models from the higher-order frequency response functions, the models obtained in almost all cases show a remarkable consistency. The structure of the continuous time models estimated for the Salford and Christchurch Bay data is of the form

$$\alpha_3 \frac{d^3 y}{dt^3} + \alpha_2 \frac{d^2 y}{dt^2} + \alpha_1 \frac{dy}{dt} + y = \beta_m \frac{du}{dt} + \beta_{d1} u + \beta_{d3} u^3 \quad (58)$$

and the model for De Voorst tube has the structure given by

$$\alpha_2 \frac{d^2 y}{dt^2} + \alpha_1 \frac{dy}{dt} + y = \beta_m \frac{du}{dt} + \beta_{d1} u + \beta_{d3} u^3. \quad (59)$$

It has been observed that although perfectly reconstructed continuous time models (sum of E values equal 100%) for Salford and Christchurch Bay data yield models possessing third-order output dynamics, the exclusion of the term $d^3 y/dt^3$ during the reconstruction phase does not significantly affect the overall performance of the model. A continuous time model of the form given in equation (59) seems to be adequate to emulate all the dynamics associated with the wave force data.

The last two terms on the right-hand side of equation (59) can be assumed to be associated with the drag term. Note that while estimating the NARMAX model, it was found that with present available data sets, a third-order NARMAX model was sufficient to model all the relevant features of the data. Hence the estimated continuous time models possesses non-linearity up to the third degree. However, depending on the different experimental conditions it may not be possible to approximate the system input–output data with a NARMAX model of third order, and the corresponding reconstructed non-linear model may contain higher-order non-linear terms of the input. To accommodate those possibilities a model structure containing an explicit drag term

$$\alpha_2 \frac{d^2 y}{dt^2} + \alpha_1 \frac{dy}{dt} + y = \beta_m \frac{du}{dt} + \beta_d u|u| \quad (60)$$

is preferred. The coefficients β_m and β_d are related to inertia and drag coefficients, respectively, such that

$$\begin{aligned} \beta_m &= 0.25\pi\rho D^2 C_m, \\ \beta_d &= 0.5\rho D C_d. \end{aligned} \quad (61)$$

Therefore, equation (60) is referred to as the dynamic Morison equation.

9.2.1. Characteristics of the dynamic Morison equation

- The linear transfer function of the proposed equation is given by

$$H_1(j\omega_1) = \frac{\beta_{d1} + j\omega\beta_m}{1 + j\omega\alpha_2 + (j\omega)^2\alpha_2}. \quad (62)$$

Thus as $\omega \rightarrow \infty$, $H_1(j\omega_1) \rightarrow 0$ implying that it does not suffer from high-frequency instability.

- The drag term $u|u|$, in conjunction with the output derivative terms can emulate the non-linear features of the system to an arbitrary degree of accuracy.

9.3. PARAMETER ESTIMATION BASED ON THE DYNAMIC MORISON EQUATION

Having postulating a new model structure [equation (60)], the next step is to estimate the parameters α_1 , α_2 , β_m and β_d . These can be estimated directly by applying a standard least squares estimator with noise modelling to the input–output data, but this involves computation of the input and output derivatives. To reduce the effects of noise due to differentiation, the parameters of the approximated form of the new model structure [equation (59)] were estimated using the reconstruction procedure described in Section 6.

9.4. SUMMARY OF RESULTS AND DISCUSSION

The results of estimating different forms of continuous time models to all the data sets are summarised in Tables 12–16. For each data set, the models fitted are as follows.

- Morison: models fitted based on the Morison equation using least squares curve fitting techniques.
- Reconstructed (NARMAX): continuous time differential equation models reconstructed by curve fitting to the GFRF using the weighted complex orthogonal estimator.
- Dynamic Morison (reconstructed): parameters of equation (59) where the $u|u|$ has been approximated by cubic estimated from the GFRF.

The predictive performance of these models together with the dynamic Morison model without history terms have been evaluated based on normalised mean square error. Terms of the form $(\beta_{d1}u + \beta_{d3}u^3)$ in the reconstructed models have been approximated by $\beta_{d1}u|u|$ in a least square sense and the drag coefficients were then calculated using equation (61).

The dynamic Morison equation (60) has two additional terms with coefficients which may be non-dimensionalised with reference to a time scale. For this purpose, the wave period associated with the peak in the spectrum (or the mid-point in the case of the Salford data) as chosen. Equation (60) is thus given by

$$\gamma_2 T_w^2 \ddot{y} + \gamma_1 T_w \dot{y} + y = \beta_m \dot{u} + \beta_d u|u|. \quad (63)$$

It is always desirable that coefficients of the equation should vary as little as possible from one situation to another and, after experimenting algebraically, equation (63) is written in the form

$$\gamma_0 (\gamma_1 T_w)^2 \ddot{y} + \gamma_1 T_w \dot{y} + y = \beta_m \dot{u} + \beta_d u|u|. \quad (64)$$

From the results for the five test situations, it can be seen that the values of γ_0 are very similar apart from Salford data set 3 which is unusual in that it has a wide band spectrum (Table 17). The narrower bandwidths for Salford data sets 1 and 2 and for the Christchurch Bay and De Voorst data have $\gamma_0 = 0.86 \pm 0.04$. This is a remarkably small variation considering the range of KC, Re and wave conditions (from unidirectional wave flumes

to directional field conditions). It is also interesting to compare the coefficients for the Salford data with those for the De Voorst flume. The KC values are similar (about 5) but the Reynolds numbers differ in magnitude by approximately a factor of 80. It is generally accepted that vortex shedding becomes weaker as Reynolds number increases [2, 30]. Vortex shedding generates the history effects and the value of $\gamma_1 \simeq 0.1$ for the Salford data ($Re \simeq 3 \times 10^3$) and $\gamma_1 \simeq 0.03$ for the De Voorst data ($Re \simeq 2 \times 10^5$). On the other hand, the Reynolds number of the De Voorst and Christchurch Bay data are similar (within a factor of 2) but the KC values are very different. At $KC = 6$ for the former vortex shedding is generally less strong than for $KC \simeq 20$ for the latter. The corresponding values of γ_1 are 0.03 and 0.06. The values of γ_1 are therefore consistent with knowledge of vortex shedding and its dependence on KC and Re.

It is also interesting to note the values of C_d and C_m . C_m varies little, but $C_d \simeq 0.4$ at high Reynolds numbers is much smaller than at the lower Reynolds numbers where $C_d \simeq 1.8$. While this overall trend with Reynolds number is expected, $C_d \simeq 0.4$ is less than what is normally obtained at $Re > 10^5$ from the Morison equation where $C_d \simeq 0.6$.

The results in terms of non-dimensional coefficients are thus quite encouraging but many more situations need to be analysed to confirm these preliminary findings.

10. CONCLUSIONS

Non-linear continuous time models have been estimated for the wave forces on fixed cylinders from a variety of flow situations using a new procedure that does not involve direct differentiation of the input–output data and performs reasonably well in all the cases. It was shown that while the Morison equation can fit the data, it generally fails to capture the underlying dynamics of the system. Although the experimental conditions for the data used in the current modelling vary considerably and no *a priori* assumptions were made regarding the structure of either the discrete NARMAX or the non-linear continuous time models during the estimation phase, the models estimated from all the data sets and the associated frequency response functions show a remarkable consistency. This suggests that there is a consistent underlying model form and a new equation called the dynamic Morison equation has been proposed. Thus, a new equation structure has been formulated from thorough mathematical analysis, experimental observation and intuitive reasoning to produce an effective model which emulates all the non-linear and dynamic features of wave force mechanisms and performs well in the prediction of wave forces. This new equation involves two non-dimensional coefficients describing history effects (one of which is almost constant) in addition to the drag and inertia coefficients of the standard Morison equation. These coefficients are consistent with the physical understanding of vortex shedding for widely different Keulegan–Carpenter numbers and Reynolds numbers.

ACKNOWLEDGEMENTS

AKS gratefully acknowledges the financial support provided by the Commonwealth Scholarship Commission of the United Kingdom and is thankful to Board of Governors, Regional Engineering College, Rourkela, India for granting study leave. SAB gratefully acknowledges that part of this work was supported by EPSRC.

REFERENCES

1. J. R. MORISON, M. P. O'BRIEN, J. W. JOHNSON and S. A. SCHAF 1950 *Petroleum Transactions* **189**, 189–202. The force exerted by surface waves on piles.
2. T. SARPKAYA and M. ISAACSON 1981 *Mechanics of Wave Forces on Offshore Structures*. Van Nostrand Reinhold.

3. S. K. CHAKRABARTI 1987 *Hydrodynamics of Offshore Structures*. Southampton: Springer-Verlag.
4. P. STANSBY, K. WORDEN, S. A. BILLINGS and G. R. TOMLINSON 1992 *Applied Ocean Research* **14**, 107–118. Improved wave force classification using system identification.
5. I. J. LEONTARITIS and S. A. BILLINGS 1985 *International Journal of Control* **41**, 303–344. Input–output parametric models for nonlinear systems, part I—deterministic nonlinear systems; part II—stochastic nonlinear systems.
6. K. WORDEN, P. K. STANSBY, G. R. TOMLINSON and S. A. BILLINGS 1994 *Journal of Fluids and Structures* **8**, 19–71. Identification of non-linear wave forces.
7. H. UNBEHAUEN and G. P. RAO 1987 *Identification of Continuous Systems*. Amsterdam: System and Control Series.
8. K. I. KIM and E. J. POWERS 1988 *IEEE Transactions of the ASSP* **36**, 1758–1769. A digital method of modelling quadratically nonlinear systems with a general random input.
9. S. A. BILLINGS and K. M. TSANG 1989 *Mechanical Systems and Signal Processing* **3**, 319–339. Spectral analysis for nonlinear systems, part I—parametric nonlinear spectral analysis.
10. J. C. PEYTON JONES and S. A. BILLINGS 1989 *International Journal of Control* **50**, 1925–1940. A recursive algorithm for computing the frequency response of a class of nonlinear difference equation models.
11. K. M. TSANG and S. A. BILLINGS 1992 *Mechanical Systems and Signal Processing* **6**, 69–84. Reconstruction of linear and non-linear continuous time models for discrete time sampled data systems.
12. A. K. SWAIN and S. A. BILLINGS 1998 *Mechanical Systems and Signal Processing* **12**, ?? Weighted complex orthogonal estimator for identifying linear and non-linear continuous time models from generalised frequency response functions.
13. G. PALM and T. POGGIO 1977 *SIAM Journal of Applied Mathematics* **33**. The Volterra representation and the Wiener expansion: validity and pitfall.
14. S. A. BILLINGS 1980 *Proceedings of the IEE* **127**, 272–285. Identification of nonlinear systems—a survey.
15. S. A. BILLINGS and I. J. LEONTARITIS 1982 *Proceedings of the 6th IFAC Symposium on Identification and System Parameter Estimation*, 505–510. Parameter estimation techniques for nonlinear systems.
16. S. A. BILLINGS, M. J. KORENBERG and S. CHEN 1988 *International Journal of System Science* **19**, 1559–1568. Identification of nonlinear output affine systems using an orthogonal least square algorithm.
17. S. A. BILLINGS and W. S. F. VOON 1986 *International Journal of Control* **44**, 235–244. Correlation based model validity tests for nonlinear models.
18. S. A. BILLINGS and Q. ZHU 1994 *International Journal of Control* **59**, 1439–1463. Structure detection for nonlinear dynamic rational models.
19. S. A. WEIGEND and N. A. GERSHENFELD 1993 *Time Series Prediction: Forecasting the Future and Understanding the Past. Proceedings of the NATO Advanced Research Workshop on Comparative Time Series Analysis held in Sante Fe, SFI studies in Sciences of Complexity XV*. Addison-Wesley.
20. T. SODERSTROM and P. STOICA 1989 *System Identification*. London: Prentice Hall.
21. R. ISERMAN 1980 *Practical Aspects of Process Identification*. Automatica.
22. L. LJUNG 1987 *System Identification—Theory for the User*. Englewood Cliffs, NJ: Prentice Hall.
23. S. A. BILLINGS and L. A. AGUIRRE 1995 *International Journal of Bifurcation and Chaos* **5**, 1541–1556. Effects of sampling time on the dynamics and identification of nonlinear models.
24. S. A. BILLINGS and J. C. PEYTON JONES 1990 *International Journal of Control* **52**, 863–879. Mapping nonlinear integro-differential equations into the frequency domain.
25. M. BAKER 1994 *Ph.D dissertation, University of Salford, U.K.* Wave loading on a small diameter flexibly mounted cylinder in random waves.
26. MATLAB 1992 *MATLAB High Performance Numeric Computation and Visualization Software: Reference Guide*. The Mathworks.
27. J. R. BISHOP 1979 *National Maritime Institute Report NMI R57*. Aspects of large scale wave force experiments and some early results from Christchurch Bay.
28. M. J. S. DAVIES, J. M. R. GRAHAM and P. W. BEARMAN 1990 In *Environmental Forces on Offshore Structures and their Prediction*, pp. 113–136, Academic Press. In-line forces on fixed cylinders in regular and random waves.
29. P. STANSBY 1977 *Proceedings of the Civil Engineers* **63**, 865–880. An inviscid model of vortex shedding from a circular cylinder in steady and oscillatory flows.
30. P. STANSBY and M. ISAACSON 1987 Recent developments in offshore hydrodynamics, a workshop report. *Applied Ocean Research* **9**, 118–127.

APPENDIX A: WEIGHTED ORTHOGONAL LEAST SQUARES

Consider a system which can be modelled as

$$z(j\omega) = \sum_{i=1}^M \theta_i p_i(j\omega) + \xi(j\omega) \quad (\text{A1})$$

where $\theta_i, i = 1, \dots, M$ are the real unknown deterministic parameters of the system associated with the complex regressors $p_i(j\omega), i = 1, \dots, M$. $z(j\omega)$ is a complex-dependent variable or the term to regress upon, and $\xi(j\omega)$ represents the modelling error. Before any attempt is made to estimate the parameters θ , the complex variables involved in equation (A1) should be partitioned in to real and imaginary parts; otherwise θ could be complex. If N measurements of $z(j\omega)$ and $p_i(j\omega)$ are available at $\omega_i, i = 1, \dots, N$ the complex system of equation (A1) can be represented after partitioning in matrix form as

$$Z = P\theta + \Xi. \quad (\text{A2})$$

The weighted complex orthogonal estimator $[n]$ transforms equation (A2) in to an auxiliary equation

$$Z = Wg + \Xi. \quad (\text{A3})$$

The properties of the matrix W are such that $W^T Q W$ is orthogonal; where Q is a positive definite weighting matrix. Further, let

$$V = W^T Q. \quad (\text{A4})$$

The regressors of the auxiliary model of equation (A3) can be obtained recursively from

$$\begin{aligned} w_1(\omega) &= p_1(\omega) \\ w_i(\omega) &= p_i(\omega) - \sum_{k=1}^{i-1} \alpha_{ki} w_k(\omega) \quad \text{for } k < i \end{aligned} \quad (\text{A5})$$

where

$$\begin{aligned} \alpha_{ki} &= \frac{\langle (w_k^T(\omega)Q), p_i(\omega) \rangle}{\langle (w_k^T(\omega)Q), w_k(\omega) \rangle} \\ &= \frac{\langle v_k(\omega), p_i(\omega) \rangle}{\langle v_k(\omega), w_k(\omega) \rangle} \quad \text{for } k = 1 \dots i-1 \end{aligned} \quad (\text{A6})$$

and $\langle ., . \rangle$ denotes the dot product of the vectors. The estimates of the i th element of the auxiliary parameter vector g is given by

$$\hat{g}_i = \frac{\langle Z(\omega), v_i(\omega) \rangle}{\langle v_i(\omega), w_i(\omega) \rangle} \quad \text{for } i = 1, \dots, M. \quad (\text{A7})$$

Once the parameters $g_i, i = 1, \dots, M$ are estimated, the original system parameters $\theta_i, i = 1, \dots, M$ can be recovered easily according to the formula

$$\hat{\theta} = \hat{g} - (T - I)\hat{\theta} \quad (\text{A8})$$

that is

$$\begin{aligned}\hat{\theta}_M &= \hat{g}_M \\ \hat{\theta}_k &= \hat{g}_k - \sum_{i=k+1}^M \alpha_{ki} \hat{\theta}_i, \quad \text{for } k = 1, \dots, M-1.\end{aligned}\tag{A9}$$

Therefore, by using the above equations, the unknown parameters θ_i , $i = 1, \dots, M$ can be estimated step by step. The structure of the system or which term to include in the model can be determined by using the error reduction ratio (test E)

$$E_i = \frac{g_i^2 \langle v_i(\omega), w_i(\omega) \rangle}{\langle (z^T(\omega)Q), z(\omega) \rangle} \times 100\%, \quad i = 1, \dots, M\tag{A10}$$

which gives the percentage contribution that each term makes to the output variance (energy). The value of E indicates the significance of a candidate term. Normally at the beginning, all available candidate terms are examined and the term which contributes the maximum E is included in the model. This is repeated until all candidate terms have been exhausted or the sum of the E reaches around 100%.